TEXAS BRAZOS RIVER FLOW AND MUSSEL GROWTH RECONSTRUCTIONS

USING STABLE OXYGEN, HYDROGEN, AND CARBON ISOTOPES AND TRACE

ELEMENTS

A Dissertation

by

ALEXANDER ANGUS VAN PLANTINGA

Submitted to the Office of Graduate and Professional Studies of
Texas A&M University
in partial fulfillment of the requirements for the degree of

DOCTOR OF PHILOSOPHY

Chair of Committee,	Ethan L. Grossman
Co-Chair of Committee,	E. Brendan Roark
Committee Members,	Franco Marcantonio
	Jason B. West
Head of Department,	Michael Pope

December 2015

Major Subject: Geology

ABSTRACT

The interaction between drought and river regulation is monitored to better understand river flow mixing, evaporation, and surface-groundwater exchange in changing regional climates and in increasingly regulated waterways. I compared Brazos River stable isotope ($\delta^{18}O$ and δD) and electrical conductivity values with reservoir, creek, and aquifer samples in the Brazos watershed, the largest watershed in Texas. Shells from two common species of Brazos River mussel, *Amblema plicata* and *Cyrtonaias tampicoensis*, were serially-sampled in the inner and outer shell layers for $\delta^{18}O$, $\delta^{13}C$, and trace elements to examine the isotopic and chemical signatures of the 2011-2014 drought. Predicted aragonite $\delta^{18}O$ for the 2012-13 study interval has an irregular pattern that complicates development of growth chronologies in modern shells. To circumvent this problem, clumped isotope (Δ_{47}) temperature measurements were used for interpreting segments of shell growth chronologies. To characterize the influence that biological and environmental variables have on shell chemistry, one specimen from each of the above two mussel species were studied using paired isotope-trace element analyses and cathodoluminescence.

The Brazos River Alluvium Aquifer and the Lake Whitney reservoir, both on the main river channel, represent water source endmembers of dilute runoff water and evaporated saline water, respectively. The difference between river and precipitation $\delta^{18}O$, or $\Delta^{18}O_{RIV-PPT}$, a measurement of degree of evaporation, ranged from 0.9‰ for a

small creek, to 2.7‰ for the Brazos River, to at least 3.7‰ in Lake Whitney. $\delta^{18}O$

values and trends were similar in coeval shell transects, indicating that $\delta^{18}O$ is a valid

chronometer when calibrated, although all shell had winter growth cessations. $\delta^{13}C$

trends were similar between shells, suggesting strong environmental control influenced

by upstream dam releases. The shell isotope chronologies can be used to reconstruct

variation in river discharge, flow source, and salinity. Shell $\delta^{13}C$, Sr/Ca, and Mn/Ca

generally covaried in the shell regions sampled, and shell $\delta^{13}C$ is thought to be

controlled by upstream dam releases based on previous work. Relationships between

Sr/Ca and temperature are consistent with temperature-paced metabolic control on shell

Sr/Ca as in other studies.

DEDICATION

To all of my Aggie and College Station friends

Guillemette and Lindsey Hunt for EPMA analyses. Mike Tice and Jian Gong helped

with XRF and 3D imaging.

TABLE OF CONTENTS

LIST OF FIGURES

LIST OF TABLES

CHPATER I

INTRODUCTION

Stable isotopes and trace elements are useful environmental tracers, particularly in catchment hydrology where fundamental questions remain about surface-groundwater interaction, storm event response, baseflow, and the impact of dam releases on hydrologic regimes. Texas endured severe drought from 2011-2014 followed by historically unprecedented flooding in May 2015. During the drought, reservoir levels plummeted and the ranching industry suffered greatly. Then, the 2014-2015 drought in the western US pushed water resources even further into the spotlight. Yet scientists are still grappling with the crucial but elusive interactions between rivers and aquifers. Water management professionals are gradually acknowledging that withdrawal from alluvial aquifers can subtract from the surface waters they drain. As populations grow in drought-susceptible regions, improved knowledge of catchment hydrology can further improve resource management practices. Extensive data sets for such variables as precipitation, discharge, well levels, and water chemistry can help build the necessary hydrologic knowledge base for better water management.

During severe droughts and floods, wildlife may get less attention, but the variables that affect Texas watersheds (precipitation, runoff, evaporation, etc.) also act on Texas aquatic species such as mussels. Stable isotopes and trace element profiles of freshwater mussel shells (sclerochronology) can be used to develop records of past river

environment, as well as elucidate mussel growth patterns and ecology. Since the 1990's, environmental destruction and invasive species competition have increasingly threatened freshwater mussels (Unionidae). Knowledge is lacking for North American freshwater mussel species morphology, reproductive patterns, growth rate and their responses to floods, droughts, and pollution. Current understanding of mussel biology and ecology is inadequate largely due to the surprising degree of individual variation in unionids (Haag, 2012).

Here I perform hydrograph separation in the Brazos River in College Station, Texas using salinity (measured as electrical conductivity), trace elements, and hydrogen and oxygen isotopes. With these tracers I identified flow components from Lake Whitney (an on-channel hydroelectric and flood-control reservoir), the Little River (a tributary), runoff, and the Brazos River Alluvium Aquifer (which provides baseflow to the river). Once I characterized their endmember values, flow components could be incorporated into a mixing model. Evaporation can also be monitored with water stable isotopes. I modeled evaporation along the main channel in order to compare evaporation in the flowing river with evaporation in Lake Whitney.

Using the record of Brazos River oxygen isotope values, I was able to develop mussel growth chronologies for specimens of common endemic freshwater mussels. However, the water isotope record predicted an irregular pattern in the mussel shells. This required the use of clumped isotope thermometry, a newer technique, to resolve seasonal growth segments in the shells. Establishing growth chronologies made the

shells useful for reconstructing river discharge, reservoir releases, and salinity. Trace element profiles in the shells (e.g, Mn/Ca, Sr/Ca) helped characterize the organism's metabolic histories, which, in some cases followed seasonal patterns. Comparing modern and historical mussel shell chemistry contributed some insight into the hydrologic effects of Lake Whitney dam.

This study contributes to our understanding of Brazos River flow and evaporation, and freshwater mussel growth during a drought. Reconstructing mussel metabolic patterns and environmental data from shells can advance our knowledge of how mussels interact with their environment. This may make mussels more useful as paleoclimate proxies for deep-time studies.

CHAPTER II

CHEMICAL AND ISOTOPIC TRACER EVALUATION OF WATER MIXING AND

EVAPORATION IN A DAMMED TEXAS RIVER DURING DROUGHT

Introduction

Watersheds in Texas, USA provide an excellent opportunity to study the

important interactions between drought and river regulation. The Texas drought that

began in 2011 caused dramatic declines in Texas cattle populations, grain production

(Kerr, 2012), tree population (Moore et al., 2013), and lake levels

(http://waterdata.usgs.gov/tx/nwis/rt). Climate change patterns are predicted to

negatively interact with growing water resource consumption in Texas (Ward, 2012).

Most major Texas rivers are dammed for flood control and hydropower. Wurbs and

Ayala (2014) estimate that evaporation from Texas reservoirs equals over half of state

agricultural water use and is more than state municipal water use. Texas river

invertebrate species are susceptible to drought (Gentner and Hopkins, 1966) and to river

regulation (Randklev et al., 2013). River regulation is known to alter water flow across

the hyporheic zone (Boulton et al., 1998; Tufenkji et al., 2002; Hucks Sawyer et al.,

2009). A manifold increase in worldwide hydropower is predicted for the next decade

(Zarfl et al., 2015). These considerations make it necessary to trace water flow paths in

regulated Texas rivers during drought. This study compares water electrical conductivity

(EC) and stable isotope data for hydrograph separation and measures of water

evaporation in the Brazos River and its tributaries in Brazos County, Texas during 2012-2013.

Both the oxygen and hydrogen isotopic composition of rain vary as a function of temperature, altitude, latitude, and distance inland (Dansgaard, 1964). Water stable isotopes can be used to trace all aspects of the water cycle (Criss, 1999), including river water origin and evaporation (Kendall and McDonnell, 1999; Kendall and Coplen, 2001; Burns, 2002; Dutton et al., 2005; Hui et al., 2007). Combining water isotopes and EC can resolve regional and seasonal water mixing patterns in rivers (Criss et al., 2001; Lambs, 2000). Surface-groundwater interaction can also be traced with water stable isotopes and dissolved ions (Fette et al., 2005). Furthermore, effects of river regulation on flows, including flow integration and evaporation in reservoirs, can also be studied with water isotopes (Gibson and Edwards, 2002; Soulsby et al., 2014). Studies that used stable isotope measurements to quantify river evaporation and trace groundwater have been performed in the Dousitu River, China (Hui et al., 2007) and in the Baron-Darling River system, Australia (Hughes et al., 2012).

Water isotope values are expressed in the following notation: $\delta_{sample}= (R_{sample} - R_{standard}) / (R_{standard}) - 1000‰$, where R is $^{18}O/^{16}O$ or D/H and the standard is Vienna Standard Mean Ocean Water (VSMOW). $\delta^{18}O$ in small groundwater-fed rivers in Texas generally decreases inland from about -2‰ near the Gulf Coast to about -10‰ in northwestern Texas (Kendall and Coplen, 2001). Generally, seasonal changes in river $\delta^{18}O$ are naturally inversely proportional to drainage area, but dams and groundwater return flows can alter this relationship. For example, Dutton et al. (2005) reported

general isotopic enrichment of Texas river water ($\delta^{18}O_{RIV}$) relative to local precipitation ($\delta^{18}O_{PPT}$), which is a consequence of surface water evaporation in Texas. Texas has 195 major surface water reservoirs (storage > 5000 acre-feet) and over 3000 minor reservoirs (200-5000 acre-feet). Assuming a direct relationship between surface water residence time and ^{18}O-enrichment, this likely increases the $\delta^{18}O_{RIV}$ - $\delta^{18}O_{PPT}$.

With a total area of 116000 km^2, 107520 km^2 in Texas, the Brazos watershed is the largest in the state. The Brazos headwaters begin in the Permian Basin. From the junction of the Salt Fork and the Double Mountain Fork, the Brazos River flows southeast a total of 1344 km to the Gulf of Mexico just south of Freeport. In the upper run, the river flows through three flood-control and hydroelectric water storage reservoirs on the main channel: Possum Kingdom Lake, Lake Granbury, and Lake Whitney (LW), successively. This study focuses on the middle run, between LW and College Station (Figure II-1). The middle run is underlain by beds of Paleogene sandstone and marl, including two major Eocene aquifers, the Trinity and Carrizo-Wilcox. This run traverses several minor aquifers including the Queen City, Sparta, and Yegua-Jackson aquifers, and the Brazos River Alluvium Aquifer (BRAA). The BRAA is composed of Pleistocene sediments, underlies the Brazos main channel, and provides baseflow (Cronin and Wilson, 1967; Munster et al., 1996; Shah et al., 2007; Turco et al., 2007; Chowdhury et al., 2010).

The stable isotope and major element chemistry of the Brazos River, the BRAA, and the oxbow lakes adjacent to the Brazos main channel have been examined by
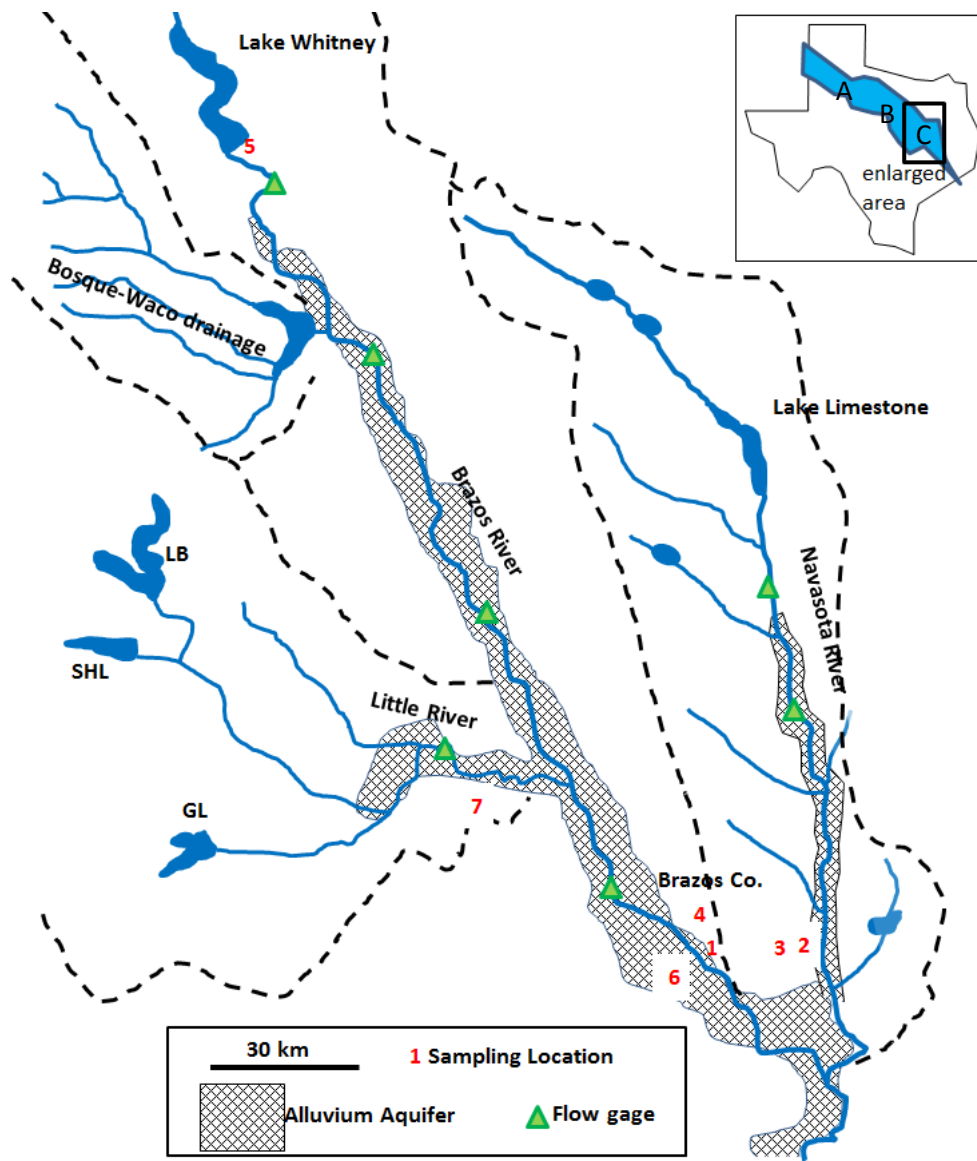
Figure II-1. Location. The middle run of the Brazos River shown in inset, from Lake Whitney to Brazos County, including drainage divides (dashed lines), major tributaries, and alluvial aquifer extent (cross-hatching). In the Texas inset: A, Permian Basin; B, Cretaceous limestone; C, Paleogene siliciclastics. Location 1 is the Brazos River at the Highway 60 bridge between Brazos and Burleson counties and the freshwater mussel sampling site, location 2 is the Navasota River at Sulpher Springs Road, location 3 is Lick Creek at Rock Prairie Road, location 4 is White Creek at FM Road 2818 and TAMU Sewage Plant Road, location 5 is Lake Whitney, location 6 is the Brazos River Alluvium Aquifer well nest, and 7 is the Little River between Cameron and Hearne. Abbreviations for Little River source reservoirs are: LB, Lake Belton; SHL, Stillhouse Hollow Lake; and GL, Granger Lake.

Chowdhury et al. (2010). Well sample data suggest that the BRAA water is relatively isotopically homogenous with $\delta^{18}O$ values similar to local rain (-4.5 to -5.2 ‰). However, BRAA TDS are highly variable along the reach of the BR. Surface water isotope data show an evaporation trend beginning at BRAA (rain) δ values and extending from the meteoric water line (MWL; $\delta D = \delta^{18}O * 8 + 10$; Craig, 1961) through the Brazos River values to the highly evaporated oxbow lake values (Chowdhury et al., 2010). Surface-groundwater interaction has also been studied using natural chemical tracers in the Bosque River basin, tributary to the Brazos River near Waco (Dworkin, 2003).

Lake Whitney is located at ~710 river miles from the confluence of the Salt Fork and Double Mountain Fork, on the main channel of the Brazos River. In the Permian Basin, high concentrations of dissolved salt from weathering halite, gypsum, limestone, and dolomite are carried downstream to the Salt Fork (Rawson, 1967). Lake Whitney receives water with a mean total dissolved solids (TDS) concentration of 927 mg/L (Wurbs and Lee, 2009). Salinity in the lake varies at seasonal or higher frequency and may vary horizontally and vertically on a scale of meters (Dunbar et al., 2008). The Little River, the largest Brazos tributary, flows by Cameron and into the Brazos in the middle run near Hearne. Lake Belton, Stillhouse Hollow Lake, and Granger Lake are major reservoirs, with storage > 5,000 acre-ft, which flow into the Little River.

Moving from northwestern Texas to the Gulf coast, the Brazos watershed climate ranges from continental steppe, to subtropical subhumid, to subtropical humid (Larkin

and Bomar, 1983). The middle Brazos run lies within the North Central Texas climate zone, which consists of hot summers and mild winters, averaging 29˚C and 13˚C, respectively (Nielsen-Gammon, 2012). Mean annual precipitation is 100 cm, and rain is normally flashy with yearly rainfall maxima occurring in May, June, and October. Rain $\delta^{18}O$ and δD in the Brazos headwaters in the Southern High Plains indicate that spring and summer precipitation tends to originate from the Gulf of Mexico and has higher δ values than winter and fall precipitation, which has a larger component of Pacific moisture (Nativ and Riggio, 1990).

Methods

Water samples were collected from the Brazos River at the Highway 60 bridge between Brazos and Burleson counties. Samples were collected weekly for 18 months from January 2012 through July 2013 using a bucket on a telescoping pole, sampling 10 cm below the water surface. Water was stored in 4 oz Nalgene bottles with headspace minimized. In order to compare isotopic response to runoff in the Brazos and small tributaries near College Station, three other streams were sampled weekly in 2012: the Navasota River at Sulphur Springs Road, Lick Creek at Rock Prairie Road, and White Creek at FM Road 2818 (Figure II-1). Lake Whitney was sampled on August 3, 2012 at 5 m depth intervals (0-27 m) by Niskin bottle near the dam and midway between the lake inlet and dam. Lake Whitney hydroelectric releases come from 7 m above lake bottom, while the waters sampled at 27 m depth in the lake, as well as samples taken

from the spillway, best reflect release water. The Lake Whitney dam released flood

pulses from the top 15 m of the water column in March, April, and September 2012. The

BRAA was sampled monthly from March-July 2013 on the Texas A&M Research Farm

adjacent to the Brazos River sampling location on Highway 60 on the Burleson County

side (Munster et al., 1996). Samples were collected from the water table well following a

purge of three well-volumes. Little River samples were collected six times between May

2013 and March 2014, on the FM Road 254 Bridge between Cameron and Hearne. Field

measurements of EC (μS/cm) were performed with a Hanna Instruments HI 8733

conductivity meter, and pH and temperature were measured with an Orion 290A unit

calibrated with pH 7 and 10 buffer solutions. Water samples were refrigerated at 10˚C

and turbid samples were filtered using 0.45 μm glass fiber filters in order to minimize

organic matter content. Samples were measured for $\delta^{18}O$ and δD using a Picarro L2120i

cavity ringdown spectrometer at the Stable Isotope Geoscience Facility at Texas A&M

University (SIGF). We determined that organic matter interference in these

measurements was minimal because 1) the Organic_Base parameter did not vary by

more than 3 ppb, and 2) we ran a subset of water samples on a Finnigan GasBench II

connected to a Finnigan DELTAplusXP isotope ratio mass spectrometer (using

VSMOW and SLAP for calibration) and the comparisons were within 0.13‰, and so

within the 0.16‰ precision guaranteed by the lab. We calibrated isotope measurements

with a one-point calibration to internal standard SIGF2013 ($\delta^{18}O$ = -4.71‰, δD = -

27.4‰), which was calibrated using VSMOW, GISP, and SLAP. Monthly water Brazos

River samples and two or more Lake Whitney and Brazos River Alluvium Aquifer

samples were analyzed at the Texas A&M University Soil Water Forage Testing Laboratory for major ions (Na^+, K^+, Ca^{2+} and Mg^{2+}, SO_4^{2-}) using ICP-MS and HCO_3^- and Cl^- using titration.

To provide a reference for endmember behavior, we made a simple isotope mass balance model of Brazos River evaporation within the 180 mile reach from LW to College Station. We treat this reach as a homogenous body of water with a uniform cross section, which, along with residence time, is approximated as a function of discharge, Q. Fraction of water evaporated, f_e, is most simply viewed in terms of volume evaporated divided by total water volume. Our model is a function of rates of flow and evaporation and is simplified as the following:

$$f_e = \text{evaporation rate / discharge} \qquad\qquad \text{(II-1)}$$

Residence time is defined as volume divided by discharge, while evaporation rate for the river is defined as local pan evaporation rate multiplied by surface area. Lower or higher discharge and wider or narrower river beds result in higher or lower evaporation rates respectively and these assumptions have been previously applied in modeling river evaporation using isotope data (Hui et al., 2007). Based on cross sections of the Brazos River at Richmond archived by the USGS (Figure II-2), river width as a function of discharge (in ft^3 per month) is approximated by the product of $137.1 * Q^{0.1004}$, while cross-sectional area is the product of $48.79 * Q^{0.4996}$. Flow data were provided by the Brazos River Authority (BRA), and evaporation data (E), based on pan evaporation, were publicly available from the Texas Water Development Board website

(http://www.twdb.texas.gov/surfacewater/conditions/evaporation/). Populating Equation

1 with these terms gives:

$$f_e = \frac{L\ (ft)\cdot W\ (ft)\cdot E\ \left(\frac{ft}{month}\right)}{Q\left(\frac{ft^3}{month}\right)} \tag{II-2}$$

Substituting the value for L (9.50 x 10^5 ft) and the equation approximating river width

(ft) as a function of discharge (ft^3/month) and factoring yields

$$f_e = \frac{9.50\ x\ 10^5\ \cdot 137.1\ Q^{0.1004}\cdot E}{Q} = 1.303\ x\ 10^8 * E * Q^{-0.9} \tag{II-3}$$

This treatment combines the contributions of the BRAA and the Little River, which

typically represents 18-35% (quartiles 1 and 3) of the Brazos River flow, based on Little

River discharge at Cameron, Texas (USGS gage no. 08106500). The Little River

receives discharge from three major reservoirs: Lake Belton, Stillhouse Hollow Lake,

and Granger Lake (Figure II-1).

The simplified Rayleigh fractionation equation estimates the change in water

isotope composition from evaporation (δ_{final} - $\delta_{initial}$ = $\Delta^{18}O_{f\text{-}i}$) as follows:

$$R = R_o * f_r^{\ (\alpha\ -\ 1)} \tag{II-4}$$

where R is the instantaneous $^{18}O/^{16}O$ ratio of the water, R_o is the initial oxygen isotope

ratio, f_r is the fraction of water remaining, and α is the equilibrium fractionation factor

between the liquid and vapor. Evaporation in nature involves both equilibrium and
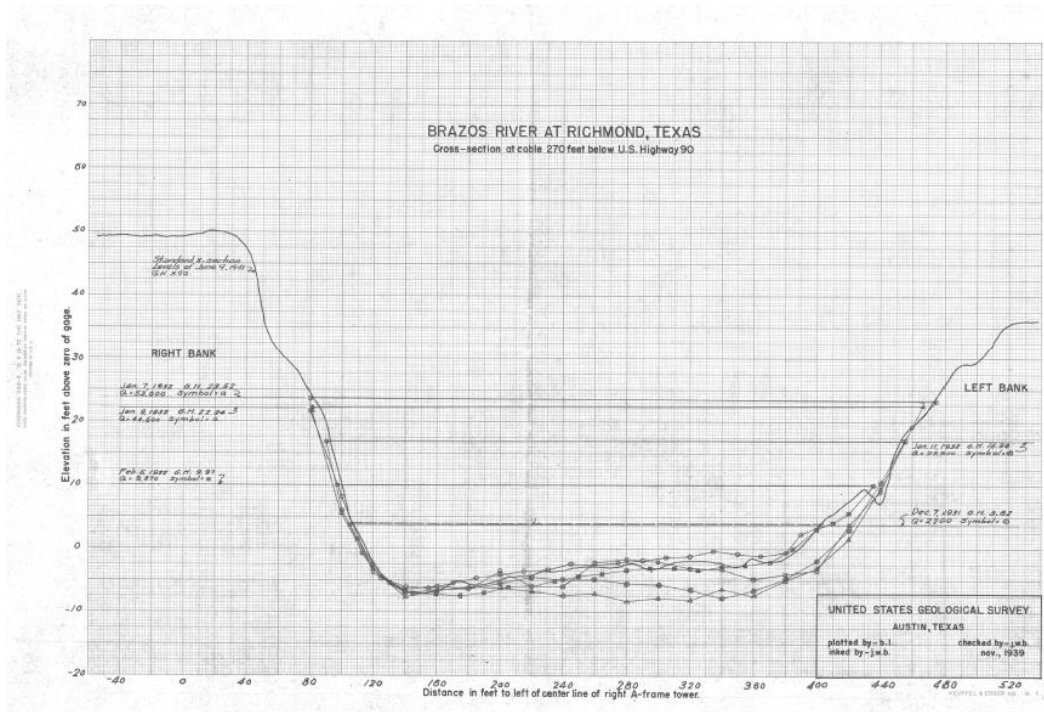
Figure II-2 Brazos River cross section rating data. Brazos River cross section and discharge provided by the USGS at the website http://txpub.usgs.gov/archives/Data.aspx?show=cs which was not accessible after April 2015 and is therefore provided here.

kinetic fractionation at the air-water interface (Craig and Gordon, 1965). The Rayleigh

model approximates maximum possible isotope enrichment in lakes from kinetic and

equilibrium effects during evaporation (Gonfiantini, 1986). In practice, researchers

divide both sides of Equation 1 by R_{VSMOW}, yielding R/R_{VSMOW} for R and R_o/R_{VSMOW} for

R_o. Equation 1 can be rewritten in δ notation as follows:

$$\delta_{final} + 1000 = (\delta_{initial} + 1000) * f_r^{\ (1/\alpha'-1)} \tag{II-5}$$

where α' is the fractionation factor that combines kinetic fractionation and equilibrium

fractionation. The enrichment in ^{18}O due to evaporation ($\Delta^{18}O_{f-i}$) of becomes

$$\Delta^{18}O_{f-i}\ (‰) = \left(\frac{\delta_{final} + 1000}{\delta_{initial} + 1000} - 1\right)1000 = (f_r^{(1/\alpha'-1)}) * 1000 \tag{II-6}$$

Model-predicted Brazos River $\delta^{18}O$ values (δ_{final}) were calculated by adding the

evaporative enrichment to a hypothetical BRAA baseflow with a $\delta^{18}O$ value of -4.9‰,

the mean for BRAA data presented in Chowdhury et al. (2010). The model outputs use

α' values that bracket extremes for isotope fractionation, with low values associated with

high temperature (35 ˚C) and 100% humidity (α' = 1.013) and high values reflecting low

temperature (5 ˚C) and 0% humidity (α' = 1.019), respectively based on relationships

from Gonfiantini (1986) and from Horita and Wesolowski (1994) (Figure II-3A). Flow

data provided by the BRA include gage data from Lake Whitney (USGS# 08092500),

computed as percent of flow at Bryan (USGS# 08108700) in Brazos County by

incorporating a three-day pressure-pulse delay factor (Chris Higgins, BRA, 2013,

personal communication). The following mixing equation for major flow sources in the

run between Lake Whitney and College Station can be used to solve for flow source, major ion composition, or, in the following format, oxygen isotope composition: rate of increase in $\delta^{18}O$ outpaces EC (Figure II-2).

In Figure II-6A the $\delta^{18}O$ and δD data show low winter (JFM) values averaging -3.9 and -25‰ for $\delta^{18}O$ and δD, respectively, which follow the MWL. High summer

$$\delta^{18}O_{BR} = f_{BRAA}\,\delta^{18}O_{BRAA} + f_{LW}\,\delta^{18}O_{LW} + f_{LR}\,\delta^{18}O_{LR} + f_{RO}\,\delta^{18}O_{RO} + \Delta^{18}O_E \qquad (II\text{-}7)$$

where f is the fraction of flow contributed and RO is the runoff component neglected here for simplicity as it is assumed to have a weighted average $\delta^{18}O$ value equivalent to the BRAA, while the evaporative enrichment $\Delta^{18}O_E$ is the average offset, 0.6‰, between the observed BR $\delta^{18}O$ in Figure II-5A and the corrected BR $\delta^{18}O$ in Figure II-5B where the modeled effect of main river channel evaporation has been removed (Table II-1). Results of this mixing equation are plotted as X's in Figure II-5A with contributions from LR and BRAA set as half of the remaining flow not contributed by LW, and they track the regression line ($p < 0.05$ for Pearson's r).

Results

Brazos River $\delta^{18}O$ and EC track each other through the study duration, and they appear to increase in the summer along with increasing LW flow as a percentage of Brazos River flow in Brazos County (FigureII-3). Plotting EC measurements against $\delta^{18}O$ demonstrates a positive correlation between EC and $\delta^{18}O$ in Brazos River water

(Figure II-4; regression information in Table II-1). Because the only BRAA samples analyzed in this study came from the Highway 60 well nest, there is a narrower range in BRAA salinity values than in Chowdhury (2004). Model-predicted Brazos River $\delta^{18}O$ values are shown as modeled minimum and maximum evaporation $\delta^{18}O$ in Figure II-3A. Measured $\delta^{18}O$ and EC values (Figures II-5A and II-5C increase with increasing LW contribution to the Brazos River in Brazos County, reported as percent of total flow. In order to model Brazos River $\delta^{18}O$ values in the absence of evaporation along the river main channel, minimum modeled $\Delta^{18}O_{f-i}$ values (Table II-2) were subtracted from observed $\delta^{18}O$ values (Figure II-5B). This produces a trend where the y-intercept more accurately represents the weighted average isotopic composition of all Brazos River water sources in this run of the river except for Lake Whitney. Minimum modeled values were used because comparison of corrected $\delta^{18}O$ versus % Lake Whitney contribution to Brazos flow (Figure II-5B) produces a coefficient of determination ($R^2 = 0.221$, $p < 0.05$), while trends produced using median and maximum modeled $\Delta^{18}O_{f-i}$ values do not produce significant trends, and, furthermore, using the lowest representative fractionation factor is justified because peak evaporation coincides with peak temperature. This correction produces a similar but 0.6‰ downward shifted trend compared with the observed data (Figure II-5B, Table II-1). The highest percent evaporation (13.6%) and thus highest $\Delta^{18}O_{f-i}$ occur during months of low average flow, and hence long residence times (Table II-2). The modeled evaporative increases relative to the $\delta^{18}O$ of BRAA (mod min/max evap $\delta^{18}O_{BRAA} = -4.9 + \Delta^{18}O_{f-i}$) are plotted in Figure II-3 where inverse relationship between river discharge and modeled $\Delta\delta^{18}O$ is apparent.

The modeled $\delta^{18}O$ under conditions of maximum evaporation only approaches observed

BR $\delta^{18}O$ in November 2012 and early February and early June 2013, times when the

(JAS) values follow an evaporative trend, sloping away to the right from the MWL, and

average -0.8 and -8‰ for $\delta^{18}O$ and δD, respectively, while fall (OND) and spring (AMJ)

values are generally intermediate (Table II-3). Statistics for standard linear regression

(IAEA, 1992) for isotope and EC crossplots show a range of slopes and y-intercepts

(Table II-1). To reduce cold winter storm influence on the comparison between LW and

Brazos River isotope data, linear regression analysis was performed separately on

Brazos River data from April-December only, and the results are within error of the LW

regression line (Figure II-6A, Table II-1). The Navasota River, Lick Creek, and White

Creek isotope data track the MWL closely with slopes of about 6.6 (Figure II-6B). Mean

$\delta^{18}O$ and δD values for these three waterways are lower than those for the Brazos River.

The average ^{18}O-enrichment of LW (-1.2‰) compared to the Brazos River (-2.2‰) is

about 1.0‰ (Table II-3). Assuming $\delta^{18}O_{PPT}$ = -4.9‰ (Chowdhury et al., 2010), the

$\Delta^{18}O_{RIV-PPT}$ is about 2.7‰ for the Brazos River and 3.7‰ for LW. For average Lick

Creek $\delta^{18}O_{RIV}$ of -4.0‰ (Table II-3), the $\Delta^{18}O_{RIV-PPT}$ is about 0.9‰. For average Little

River $\delta^{18}O_{RIV}$ of -2.3‰, the $\Delta^{18}O_{RIV-PPT}$ is about 2.6‰. As the Piper plot (Figure II-7)

shows, cations vary mostly in the proportions of Na^+ and Ca^{2+} and anions in the

proportions of Cl^- and HCO_3^-. Lake Whitney water conforms to Na^+-Cl^- -type water,

while Lick Creek, White Creek, and the Navasota River conform to Na^+-HCO_3^- type

water. Run of river (ROR) water conforms to Ca^{2+}-HCO_3^--type water from the BRAA

and runoff draining Central Texas Cretaceous limestones, represented by Little River
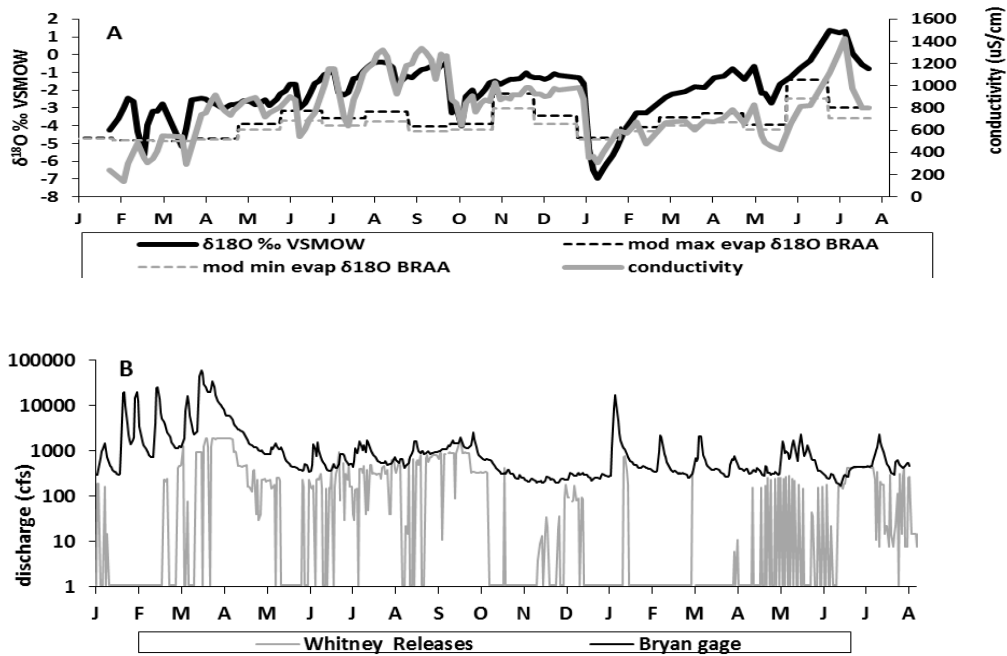
Figure II-3. River data time series. Figure II-3A. The 2012 and 2013 time series for observed $\delta^{18}O$ (thick black) and conductivity (thick gray) in the Brazos River at Bryan. The dashed lines are the minimum and maximum estimated $\delta^{18}O$ of river water based on a simple model assuming all evaporation takes place in the main channel of the river. Figure II-3B. Bryan and Lake Whitney hydrograph.
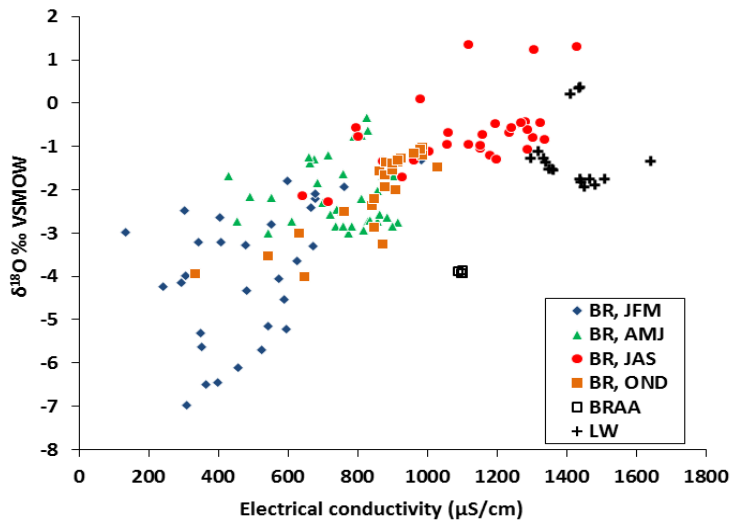
Figure II-4. Seasonal EC and $\delta^{18}O$ for the Brazos River, LW and BRAA.

18
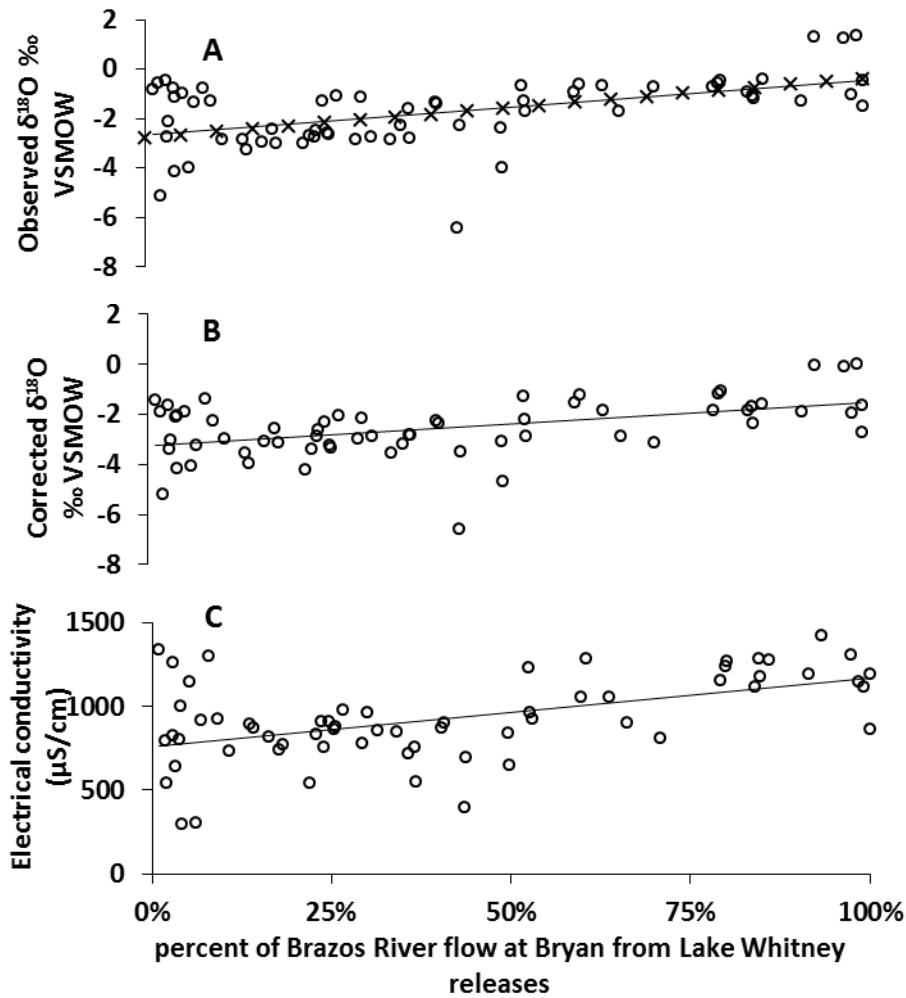
Figure II-5 Lake Whitney flow percentage, $\delta^{18}O$, conductivity plots. Figure II-5A. The relationship between Lake Whitney contribution to river flow (%LW) and observed $\delta^{18}O$ is shown with the regression line. Regression statistics in Table II-1. X's are the calculated $\delta^{18}O_{BR}$ using the Brazos River mixing equation (Equation II-7 in the Discussion). Figure II-5B. The relationship between Lake Whitney contribution to river flow and $\delta^{18}O$ as modeled by correcting for run-of-river evaporation is shown with the regression line. Regression statistics in Table II-1. Figure 5C. The relationship between LW contribution to river flow and EC is supported by the crossplot and regression statistics in Table II-1.

TABLE II-1. RIVER FLOW AND CHEMISTRY REGRESSION STATISTICS. THIS COVERS DIFFERENT SITES, DATES, AND VARIABLES. BRAZOS RIVER DATA FROM 2003 (C04) IS FROM CHOWDHURY (2004). ALL REGRESSION p VALUES < 0.05 EXCEPT FOR *.

Location	Date	x	y	m	b	Sm	Sb	R^2	N
Brazos River	2012-2013	$\delta^{18}O$	δD	5.56	-2.92	0.15	0.41	0.91	123
Brazos River	2012-2013	EC	$\delta^{18}O$	0.0043	-5.56	0.0003	0.28	0.58	119
Brazos River	JFM2012&2013	$\delta^{18}O$	δD	6.93	2.22	0.36	1.48	0.93	30
Brazos River	AMJ2012&2013	$\delta^{18}O$	δD	4.03	-4.40	0.19	0.42	0.93	36
Brazos River	JAS2012&2013	$\delta^{18}O$	δD	3.68	-5.26	0.23	0.26	0.90	29
Brazos River	OND2012	$\delta^{18}O$	δD	7.03	-1.60	0.21	0.40	0.98	21
Brazos River	Apr-Dec '12	$\delta^{18}O$	δD	4.30	-4.99	0.26	0.51	0.79	72
Lake Whitney	2012-2013	$\delta^{18}O$	δD	4.37	-5.02	0.10	0.15	0.99	15
Lake Whitney*	2012-2013	EC	$\delta^{18}O$	-0.0006	-0.32	0.0023	3.30	0.01	15
Brazos River	2003	$\delta^{18}O$	δD	4.27	-11.05	0.28	0.77	0.94	16
Navasota River	2012-2013	$\delta^{18}O$	δD	6.55	2.52	0.22	0.73	0.88	122
Brazos River	2012-2013	%Q LW	$\delta^{18}O$ observed	2.18	-2.65	0.49	0.3	0.248	61
Brazos River	2012-2013	%Q LW	$\delta^{18}O$ corrected	1.69	-3.24	0.41	0.2	0.215	61
Brazos River	2012-2013	%Q LW	EC	411.09	759	87.89	46	0.264	61
Lick Creek	Jan-Sep,2012	$\delta^{18}O$	δD	6.67	7.14	0.26	1.07	0.90	69
White Creek	Jan-Sep,2012	$\delta^{18}O$	δD	6.63	5.61	0.18	0.63	0.95	74
Brazos River	2012-2013 bimonthly	Na^+/Ca^{+2}	$\delta^{18}O$ observed	1.01	-4.74	0.13	0.35	0.65	33
Brazos River	2012-2013 bimonthly	Cl^{+2}/HCO_3^-	$\delta^{18}O$ observed	1.54	-3.89	0.31	0.38	0.43	33

TABLE II-2. EVAPORATION MODEL INPUT AND OUTPUT. THIS INCLUDES
AVERAGE DISCHARGE (Q), PAN EVAPORATION (E), AND ESTIMATED RESIDENCE
TIME, EVAPORATED VOLUME, AND % EVAPORATION.

	input		output				
date	Q, ft^3/ month	E, ft/ month	monthly residence time	E, acre-ft/month	% evap	min $\Delta^{18}O_{f\text{-}i}$ ‰	max $\Delta^{18}O_{f\text{-}i}$ ‰
January '12	5.88E+09	0.24	0.37	1573	1.2	0.15	0.22
February	1.47E+10	0.23	0.24	1610	0.5	0.06	0.09
March	3.66E+10	0.31	0.15	2398	0.3	0.04	0.05
April	1.35E+10	0.43	0.24	3038	1.0	0.13	0.18
May	2.19E+09	0.45	0.61	2614	5.2	0.68	1.00
June	1.56E+09	0.56	0.72	3185	8.9	1.20	1.74
July	2.22E+09	0.59	0.61	3483	6.8	0.91	1.32
August	2.01E+09	0.68	0.64	3965	8.6	1.15	1.67
September	3.19E+09	0.55	0.51	3366	4.6	0.61	0.88
October	1.74E+09	0.37	0.68	2109	5.3	0.70	1.01
November	6.02E+08	0.36	1.16	1878	13.6	1.87	2.72
December	6.94E+08	0.23	1.08	1188	7.5	0.99	1.45
January '13	5.01E+09	0.19	0.40	1238	1.1	0.14	0.20
February	1.52E+09	0.27	0.73	1524	4.4	0.57	0.83
March	1.42E+09	0.40	0.76	2273	7.0	0.93	1.35
April	1.08E+09	0.38	0.87	2053	8.3	1.11	1.61
May	2.34E+09	0.46	0.59	2729	5.1	0.67	0.97
June	8.45E+08	0.62	0.98	3316	17.1	2.41	3.50
July	1.71E+09	0.67	0.69	3856	9.8	1.33	1.93

TABLE II-3. AVERAGE ISOTOPIC COMPOSITIONS OF LOCAL WATERS. BRAZOS RIVER 2012-2013 δ^{18}O AND δD SUMMARY WITH SEASONAL MEANS, STANDARD DEVIATIONS, MINIMA, AND MAXIMA. THE LOWER SECTION COMPARES ALL BRAZOS RIVER (BR), LAKE WHITNEY (LW), NAVASOTA RIVER (NR), LICK CREEK, AND WHITE CREEK ISOTOPE DATA MEANS AND STANDARD DEVIATIONS.

BR, season	variable	μ	σ	Min	max	
JFM	δ^{18}O, δD	-3.9, -25	1.5, 11	-7, -49	-1.3, -11	
AMJ	δ^{18}O, δD	-2.1, -13	0.8, 4	-3, -18	-0.3, 0	
JAS	δ^{18}O, δD	-0.8, -8	0.9, 3	-2.3, -13	1.3, 0	
OND	δ^{18}O, δD	-1.8, -14	0.8, 5	-4, -30	-1, -10	
variable	BR all	LW	NR	Lick	White	Little River
δ^{18}O μ, σ	-2.2, 1.5	-1.2, 0.8	-3.1, 1.1	-4.0, 0.6	-3.3, 1.3	-2.3, 1
δD μ, σ	-15, 9	-10, 3	-18, 7	-20, 4	-10, 3	-15, 6
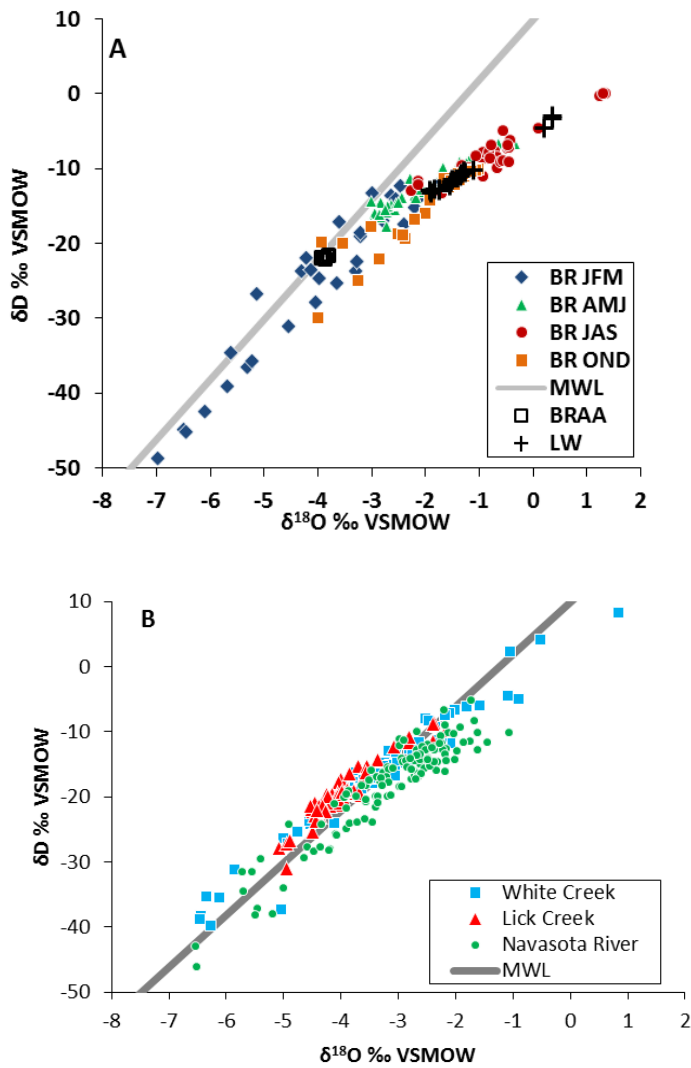
Figure II-6A. Brazos River δ¹⁸O vs. δD. Colored symbols are Brazos River samples broken down by season. Blue diamonds are winter (January, February, March) 2012 and 2013 samples, green triangles are spring (April, May, June) 2012 and 2013 samples, red circles are summer (July, August, September) 2012 and 2013 samples, and orange squares are fall (October, November, December) 2012 samples. Open squares are Brazos Alluvium Aquifer samples, crosses are Lake Whitney samples. Figure II-6B. This plot shows the δ¹⁸O vs. δD data for the Navasota River (blue squares), Lick Creek (red triangles), and White Creek (green circles) in Brazos County for 2012.
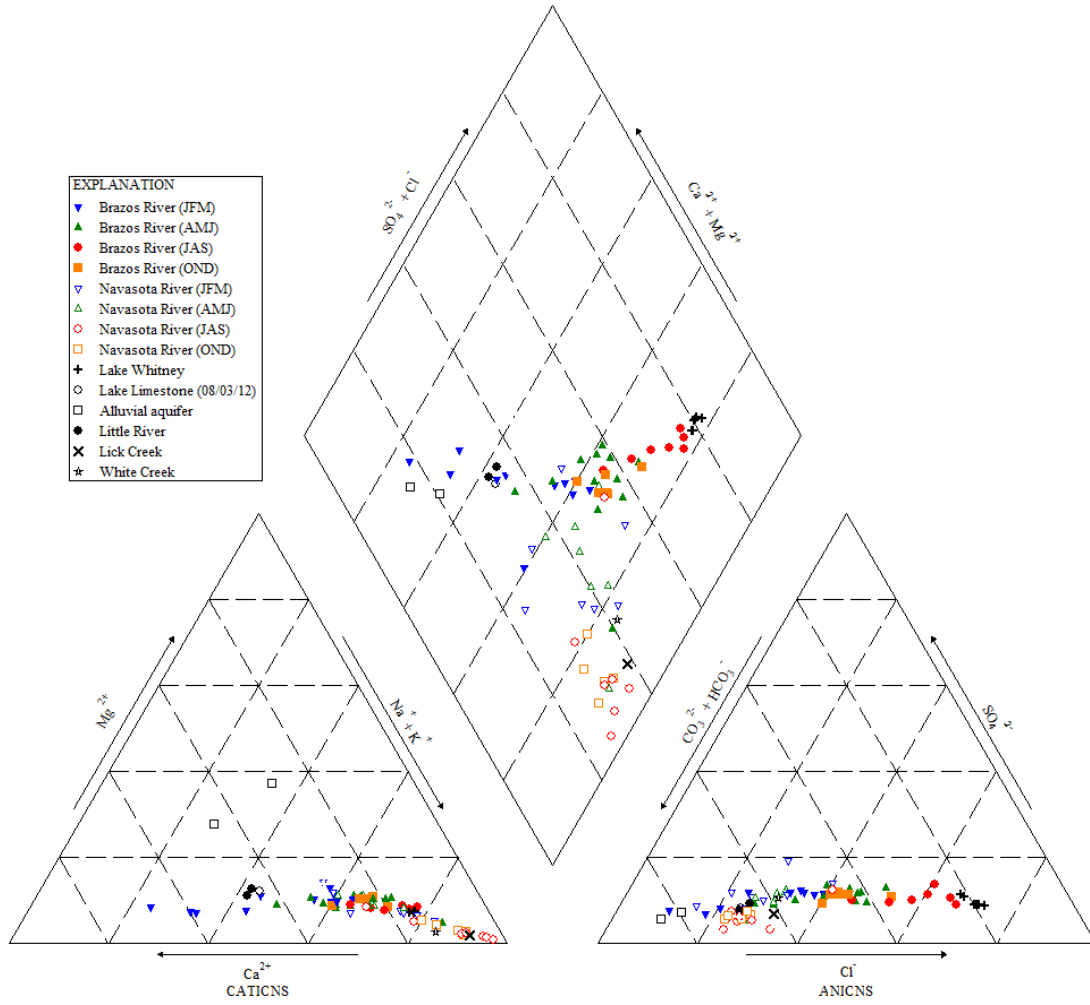
Figure II-7. Piper plot of waters analyzed.

and Lake Limestone samples. This reflects the lithologies of the upper and middle Brazos watershed. Plotting molar ratios of Na^+/Ca^{2+} against $\delta^{18}O$ (Figure II-8A) and Cl^-/HCO_3^- against $\delta^{18}O$ (Figure II-8A) depicts Permian Basin-derived LW water and BRAA water as endmembers. Based on flows in and out of LW (http://www.swf-wc.usace.army.mil/whitney/), the LW residence time for the study duration was estimated at ~2 yrs. Sulfate reduction in river reservoirs above and including LW may explain the low SO_4^{2-} concentrations in the middle Brazos River in relation to values observed in streams within the Permian basin (Nicot et al., 2007).

Discussion

Both EC and $\delta^{18}O$ are generally interpreted as tracers of two-end-member mixing of LW and ROR flows. Molar ratios of Na^+/Ca^{2+} (Figure II-8A) and Cl^-/HCO_3^- (Figure II-8B) plotted against $\delta^{18}O$ supports the endmember assumptions about Brazos watershed lithologies (Figure II-1 inset). The strong convergence of the LW data to the Brazos River (April-December) $\delta^{18}O$-δD trend reflects evaporation and water mixing (Figure II-6A and Table II-1). Lake Whitney flows dominate the Brazos River hydrograph most during summer months when hydropower production is high.

The simple isotope balance model suggests that ROR evaporation is greater at times when low total discharge and low LW discharge coincide, and this may characterize episodic gaining stream conditions in the Brazos River between Lake Whitney and Brazos County. In January 2013, where the model predicts higher $\delta^{18}O$
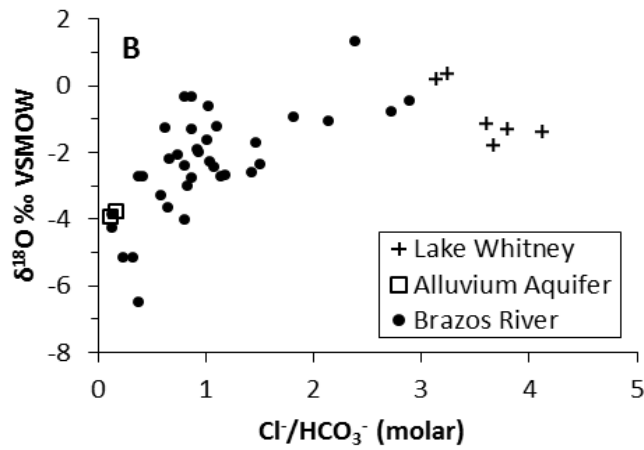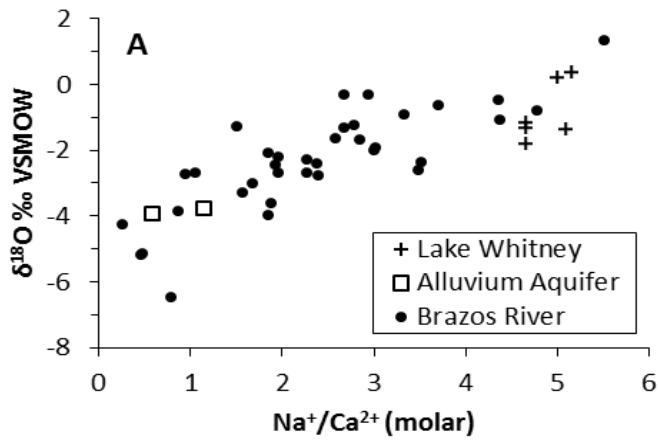
Figure II-8. Dissolved ion data vs. δ^{18}O. Figure II-8A. Molar cation ratios and bimonthly oxygen isotope measurements from the Brazos River, Lake Whitney, and the Brazos River Alluvium Aquifer. Figure 8B. Molar anion ratios and bimonthly oxygen isotope measurements from the Brazos River, Lake Whitney, and the Brazos River Alluvium Aquifer.

than observed, heavy rainfall at low temperature provided very low-δ^{18}O runoff to the river, consistent with general observations in the United States Midwest where low-δ^{18}O winter precipitation drives strong seasonal δ^{18}O trends (Dutton et al., 2005). For most of the study period observed δ^{18}O was greater than modeled δ^{18}O which is largely because Lake Whitney flow, which was not part of the simple, groundwater-based model, is a nearly constant source of high δ^{18}O water to the middle and lower Brazos River. The BRAA makes a greater contribution to Brazos River flow further downstream of Brazos County near Hempstead (Chowdhury et al., 2010). While drought conditions in unregulated rivers in general are expected to decrease discharge and increase E-P and baseflow from adjacent alluvial aquifers, regulated rivers such as the Brazos River can be dominated by reservoir flows in the hottest, driest months of the year (Figure II-3), thereby potentially suppressing alluvium aquifer baseflow.

The differences between the y-intercepts in Figure II-5A (-2.7‰) and Figure II-5B (-3.3‰, as listed in Table II-1) and the baseflow value of -4.9‰, are roughly the $\Delta^{18}O_{RIV\text{-}PPT}$ values. These values are 2.2‰ and 1.6‰, respectively. The former value (2.2‰) is the hypothetical evaporative enrichment in the main river channel, correcting for LW water contribution. The latter value (1.6‰) may be the difference between the Little River (LR) δ^{18}O and BRAA δ^{18}O, or the $\Delta^{18}O_{RIV\text{-}PPT}$ of the LR. Back-calculating the LR average δ^{18}O with this value gives an average LR δ^{18}O of -3.3‰, which is 1‰ less than the measured average LR δ^{18}O of -2.3‰. This discrepancy may result from error in the regression equation for Figure II-5B. The y-intercept in Figure II-5C indicates that EC of baseflow and tributary flow in this study was ~759 µS/cm,

compared with average LR EC of 508 µS/cm. Either the combined minor tributaries' and BRAA's salinity are on average greater than in the LR, or LR EC measurements are not representative. This requires future investigation.

Large on-channel reservoirs with residence times > 1 yr, like LW, may enhance the atmospheric influence on river chemistry, as with CO_2 exchange inferred from $\delta^{13}C_{DIC}$ (Zeng et al., 2011). We could not make steady state assumptions for modeling evaporation in LW because lake volumes fluctuate throughout the year, staying well below the minimum 10^9 m^3 volume that Gibson and Edwards (2002) designated for applying steady state assumptions in their study. Also, LW inflows contain a flow component of pre-evaporated water from Lake Granbury that does not represent $\delta^{18}O$ of local precipitation, an important variable in lake evaporation models (Gibson and Reid, 2010). However, it may be possible to correct for these conditions in future studies aimed at quantifying lake evaporation in the study area. Seasonal flow integration from different tributaries into LW will need to be better constrained in future studies (Dunbar et al., 2008). Evaporation and precipitation data for LW are available from the US Army Corps of Engineers, which can aid in critical assessment of isotope-based models.

In contrast to the Brazos River, isotope data for White Creek, Lick Creek, and the Navasota River reflect groundwater dominance. However, Lick Creek, White Creek, and the Navasota River receive discharge from wastewater treatment plants upstream of the sampling sites in this study. These municipal waters are supplied from the Carrizo-Wilcox aquifer. Water in the Carrizo-Wilcox Aquifer is early Holocene to Late

Pleistocene in age (Castro et al., 2000). The lower δ^{18}O and δD averages and standard deviations in these waterways compared with the Brazos River (Table II-2) conform to observations of river isotope values similar to local rain by Kendall and Coplen (2001). The elevated Δ^{18}O$_{RIV-PPT}$ of 0.9-2.6‰ observed in the study area was similarly noted by Dutton et al. (2005) for Texas surface waters. Dams on the Brazos River probably contribute to this observation (Figure II-4A) by increasing river transit times (Soulsby et al., 2014). Deep groundwater discharged into Lick Creek, White Creek, and the Navasota River may simulate baseflow, however this can make their assessment as natural systems using δ^{18}O difficult.

As Texas water supply reservoir levels did not fully recover from 2011 severe drought levels until 2015 (http://waterdatafortexas.org/reservoirs/statewide), and as state population growth continues, surface water budgeting is of great concern. Surface water management practices may benefit from studies such as this one that use chemical tracers to track reservoir flows and evaporation rates. Future research detecting Ra and Rn levels in the Brazos River could further elucidate groundwater fluxes (Swarzenski et al., 2007).

Conclusions

The Lake Whitney and Brazos River (April-December) isotope data fall on a regression line that is both an evaporation line and a mixing line. Isotope data and modeling from Brazos River water, combined with flow data, indicate that gaining stream conditions are more likely during low flow with low LW contributions to flow.

Modeled evaporative Δ^{18}O and measured δ^{18}O of Lake Whitney, the Little River, and the

Brazos Alluvium Aquifer (measured previously by Chowdhury et al., 2010) are well

constrained for estimating flow contributions from these components using a basic

mixing equation (Equation II-7). Brazos River isotope values suggest that significant

evaporation can take place in the flowing main channel portion of a river. Peak drought

conditions may accentuate reservoir discharge dominance in regulated rivers when

baseflow dominance would be expected in a similar undammed river. Estimates of

Δ^{18}O$_{RIV\text{-}PPT}$ ranged from 0.9‰ for a small creek, to 2.7‰ for a large river, to 3.7‰ in

Lake Whitney. This is consistent with previous research on Δ^{18}O$_{RIV\text{-}PPT}$ in North

America (Kendall and Coplen, 2001; Dutton et al., 2005).

CHAPTER III

STABLE AND CLUMPED ISOTOPE SCLEROCHRONOLOGIES OF MUSSELS

FROM THE BRAZOS RIVER, TEXAS: ENVIRONMENTAL AND ECOLOGIC

PROXY

Introduction

Sclerochronology is the science of reconstructing environmental and growth history from invertebrate hard parts such as mollusk shells or corals. Freshwater mussel (Unionidae) shells hold promise as environmental recorders, depositing layers of shell calcium carbonate that can reflect environmental conditions such as temperature, water oxygen and dissolved inorganic carbon (DIC) isotopes, food availability, salinity, and river discharge (Dettman et al., 2004; Carroll et al., 2006; Goewert et al., 2007; Versteegh et al., 2010a; Versteegh et al., 2010b). While $\delta^{18}O$ in shell growth layers is widely used to reconstruct shell growth chronology, shell $\delta^{13}C$ is sometimes but not always a reliable environmental chronicle because of metabolic effects on shell carbon isotope composition. Furthermore, combining information from assemblages of shells spanning decades or centuries can provide an extended composite record (Schöne et al, 2003). Variable growth rates, seasonally or ontogenetically and growth hiatuses complicate the use of shell growth layers as environmental records. Also sudden stress may cause non-periodic disturbance ring deposition in shells (Haag and Commens-Carson, 2008).

Stable isotopes are useful for assigning mussel growth chronologies, especially in temperate climates (Dettman et al., 1999; Versteegh et al., 2010a). Water oxygen isotopes ($\delta^{18}O_{WATER}$) have a direct effect on shell $\delta^{18}O$ ($\delta^{18}O_{SHELL}$). The $\delta^{18}O_{WATER}$ equilibrates with $\delta^{18}O$ of the HCO_3^- that converts to shell CO_3^{2-}. Temperature of mineralization is the second dominant control, with higher $CaCO_3$ $\delta^{18}O$ at low temperatures and lower $\delta^{18}O$ at high temperatures (~-1‰ per 5˚C; Epstein et al., 1953; Grossman and Ku, 1986). Thus, it is preferable to examine shells grown in environments where one of these opposing effects is constrained – for example in temperate freshwater or in marine settings where seasonal snowmelt or temperature extremes, respectively, can impart distinct annual cyclicity in the shell isotope record (Dettman and Lohmann, 1993). Paleoclimate interpretations of carbonate $\delta^{18}O$ often hinge on distinguishing between the effects of temperature and water $\delta^{18}O$ (e.g., Ivany et al., 2004). Estimating shell growth temperature based on multiply substituted isotopes, or "clumped isotopes", resolves the ambiguity between water $\delta^{18}O$ and temperature. Clumped isotope techniques have recently been introduced to resolve ambiguous shell $\delta^{18}O$ values in marine bivalves (Keating-Bitonti et al., 2011). This technique has not yet been used to study freshwater mussels (Unionidae) for constraining growth temperature and $\delta^{18}O_{SHELL}$. As for carbon isotopes ($\delta^{13}C$), aquatic mollusk shell carbon comes from DIC that may reflect watershed lithology, air-water exchange, and respired CO_2, further modified by metabolic effects on carbonate ions incorporated into the shell during biomineralization (McConnaughey and Gillikin, 2008).

Investigations into unionid shell chemistry and the environmental signals the shells record in the form of chemical chronologies can provide insights that malacologists need to better characterize mussel growth patterns, metabolic activity, and responses to environmental variables such as river discharge, temperature, and reproductive investment. Unionids are regarded as imperiled world-wide (Lydeard et al. 2004). One threat to freshwater mussel populations is dams, which alter river discharge, sediment loads, and water temperature regimes (Richter et al. 1997). Damming of rivers accounts for the 195 major reservoirs (> 5,000 acre-ft) in the state of Texas (Ward, 2012). Such damming alters mussel species composition by fragmenting habitats for mussels and host fish (Randklev et al., 2013). The Brazos is the largest river in Texas and is regulated by dams on its main channel and tributaries. Freshwater mussel populations in the Brazos watershed have been shown to decline with increasing proximity to dams (Randklev et al., 2013).

In this study, I used high-resolution stable isotope analyses, along with clumped isotopes to reconstruct shell growth chronologies in two common species of freshwater mussel, Tampico Pearlymussel (*Cyrtonaias tampicoensis*) and Threeridge (*Amblema plicata*), collected from the Brazos River near College Station, Texas. Using common species makes this study easier to reproduce. Sclerochronologies were developed based on $\delta^{18}O$ values predicted from coeval isotope and temperature data for Brazos River water, and were evaluated for their use in reconstructing river discharge. Lastly, a Threeridge mussel from the study area, collected from between 1880 and 1920, prior to major dam construction in the Brazos watershed, was evaluated using the same

techniques to contrast isotope signals and thus hydrologic conditions before and after the influence of impounded water on Brazos River oxygen isotope signatures.

Methods

The study site on the Brazos River near College Station, Texas is about 130 miles north of Freeport, where the Brazos flows into the Gulf of Mexico (Figure II-1). This study focuses on the middle Brazos run, flowing southeast through a semi-arid to semi-humid climate characterized by hot summers and mild winters, averaging 29˚C and 13˚C, respectively (Nielsen-Gammon, 2012). Average annual rainfall is 100 cm, flashy, and historically peaks in late-spring and mid-fall. About 240 km upstream of the study site is Lake Whitney, dammed for hydropower and flood control. About 30 km upstream of the study site is the confluence with the Little River, the largest Brazos tributary, receiving flows from Lake Belton, Stillhouse Hollow Lake, and Granger Lake, all dammed reservoirs.

From January 2012 through July 2013, weekly temperature measurements and water $\delta^{18}O$ samples were collected from the Brazos River at the Highway 60 bridge between Brazos and Burleson counties. Samples were measured for $\delta^{18}O$ and δD using a Picarro L2120i cavity ringdown spectrometer at the Stable Isotope Geoscience Facility at Texas A&M University (TAMU). Calibrations are described in CHAPTER II. Brazos River discharge data from the gage at Highway 21 near College Station (USGS 08108700) were obtained online from http://waterdata.usgs.gov/tx.

Temperature and water $\delta^{18}O$ data, along with the aragonite oxygen isotope thermometry equation from Dettman et al. (1999; based on Grossman and Ku, 1986), were used to predict shell $\delta^{18}O$ values, based on temperature (T) in Kelvin and $\delta^{18}O$ water in VSMOW ($\delta^{18}O_{WATER}$), as follows:

$$1000 \ln(\alpha) = 2.559 (10^6 T^{-2}) + 0.715 \qquad \text{(III-1)}$$

$$\alpha \frac{ARAGONITE}{WATER} = \frac{(1000 + \delta18O ARAGONITE)}{(1000 + \delta18O WATER (VSMOW))} \qquad \text{(III-2)}$$

$$\alpha \frac{VSMOW}{VPDB} = 1.0309 \text{ (Gonfiantini et al., 1995).} \qquad \text{(III-3)}$$

Four modern specimens each of *Amblema plicata* and *Cyrtonaias tampicoensis* were collected on August 9, 2013 from the Brazos River near the Highway 60 bridge, from a muddy to sandy bank margin habitat at depths shallower than 2 m. Two historical specimens, *A. plicata* and *C. tampicoensis*, both mature adults and labelled H3R and HTP, respectively, were borrowed from the Singley Collection from the University of Texas at Austin Non-Vertebrate Paleontology Lab. These specimens were collected between 1880 and 1920 in the Brazos River near Bryan-College Station. Mussels were aged by counting dark growth bands based on age estimation techniques from Neves and Moyer (1988). Mussel ages upon death were approximately 3-7 years old for the four modern specimens and 12 years old for the historical specimens.

I selected two specimens each, at random, of modern young adult *A. plicata* (labelled 3R5 and 3R3) and *C. tampicoensis* (TP2 and TP3) and the two historical

specimens for isotope analyses. Except for HTP, specimens were sectioned; the sectioned shells were then broken in two and epoxied to glass slides (Figures III-3A and III-3B). Shell powder samples were collected with a New Wave micromill using a 0.5 mm drill bit following the methods of Dettman and Lohmann (1995). In each shell two transects were sampled: one across the ventral margin area (also referred to as the outer nacreous layer or ONL), and one across the INL area (inner nacreous layer, or INL) near the hinge of the shell (Figure III-2). In specimen HTP, we analyzed duplicates of bulk nacreous powder drilled from a cross section of the ventral margin. Sample intervals were between 60 and 140 μm, with generally shorter spacing for INL than ONL. For isotopic analyses, ~60 μg of powder were reacted with "100%" orthophosphoric acid in a Kiel IV carbonate instrument and the CO_2 analyzed on a Thermo Finnigan MAT 253 mass spectrometer at the Stable Isotope Geosciences Facility at Texas A&M University (TAMU). Average analytical precision was 0.05‰ for $\delta^{18}O$ and 0.03‰ for $\delta^{13}C$ based on replicates of the NBS-19 internal lab standard used in every lab run.

In order to assign temperatures to shell growth intervals and determine the differences, if any, between light and dark growth layers, clumped isotope samples were taken from distinct light and dark bands within the micromilled ventral margin transects in specimens 3R5 and TP2. For clumped isotope sampling, shell periostracum was removed with sandpaper, whereas micromilling involved drilling trenches to isolate nacreous shell to be microsampled, thereby avoiding periostricum. Samples were taken from the top of the shell parallel to growth bands using a Dremel drill with a 0.5 mm dental bur on a low speed setting (Figures III-1E, F, and G). Samples were analyzed for
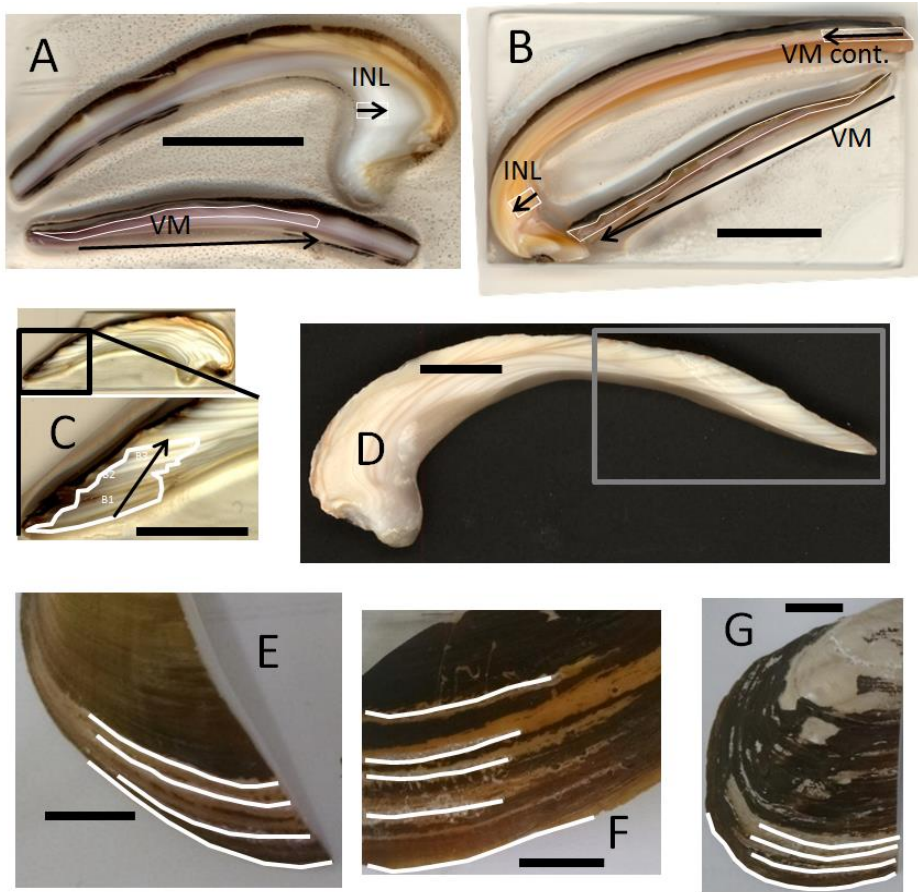
Figure III-1. Mussel shell images. Figure III-1A and III-1B are specimens 3R5 and TP2, respectively. Specimens are sectioned, broken in two pieces and fixed to glass slides; scale bar is 1 cm; micro-sampling transects are outlined in white; arrows indicate direction of sampling, VM stands for ventral margin. Figures III-1E, III-1F, and III-1G depict the clumped isotope sample regions, outlined in white, in specimens 3R5 and TP2, respectively, scale bars are 1 cm. The ventral margin clumped isotope sample was taken from the opposite side of the shell.

$\delta^{13}C$, $\delta^{18}O$ and Δ_{47} at Johns Hopkins University (JHU) during March 2015. A custom automated acid-digestion and sample purification line was used with a common acid bath of "100%" orthophosphoric acid at 90 ˚C. The line was connected to a Thermo Scientific MAT 253 mass spectrometer. Henkes et al. (2013) provides more details of this method. Three to four replicate analyses of about 8 mg each were performed per growth layer sampled.

Internal clumped isotope standards and reference gases from Jan 21-April 12 2015 were used for quality assurance and reference frame purposes. Daily isotope measurements of CO_2 gases equilibrated at 30 ˚C and 1000 ˚C were performed to make a Δ_{47} transfer function in an absolute reference frame known as the carbon dioxide equilibrium scale (Dennis et al., 2011). Raw $\delta^{18}O$ and $\delta^{13}C$ data were calibrated to the VPDB scale using NBS-19. Two internal standards were used daily to monitor performance: 102-GC-AZ01 (n = 33) with Δ_{47}, $\delta^{18}O$, and $\delta^{13}C$ of 0.697 ± 0.029‰, -14.46 ± 0.09‰, and 0.45 ± 0.06‰, respectively; and HAF-Carrara (n = 19) with Δ_{47}, $\delta^{18}O$, and $\delta^{13}C$ of 0.398 ± 0.010‰, -1.80 ± 0.03‰ and 2.29 ± 0.01‰, respectively. For paleotemperatures, we used the equation for mollusk and brachiopod shells presented in Henkes et al. (2013):

$$\Delta_{47} = 0.0327 * 10^6 / T^2 + 0.3286 \qquad\qquad \text{(III-4)}$$

Results

Water $\delta^{18}O$ and water temperature are reported in CHAPTER II and in Figure

III-2A. $\delta^{18}O$ ranges from -7.0 to 1.4‰, and temperature ranges from 6.7 to 37.8 ˚C.

Temperature and $\delta^{18}O$ covary strongly but not highly deterministically ($r^2 = 0.28$, $N =$

120, $p < 0.05$). This is a reflection of increased effects of evaporation in the summer

covarying with the increased influence of evaporated ^{18}O-enriched Lake Whitney flows

in the summer time, whereas precipitation and runoff with a lower $\delta^{18}O$ are more

dominant flow components in the winter (Chowdhury et al., 2010; CHAPTER II).
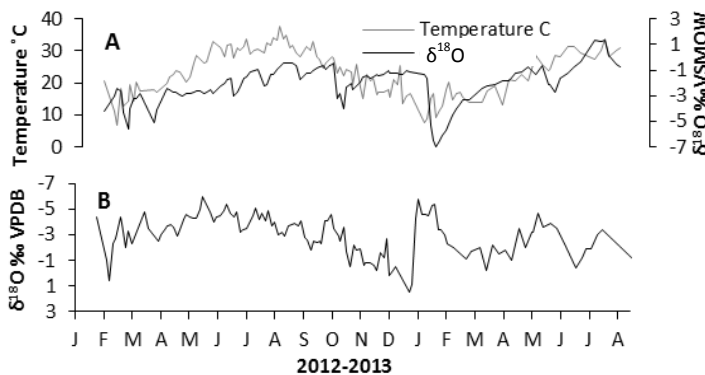
Figure III-2. Brazos River water $\delta^{18}O$, temperature, predicted aragonite $\delta^{18}O$. Figure III-2A. Water $\delta^{18}O$ and temperature from the Brazos River at Highway 60 near College Station for 2012-2013. Figure III-2B $\delta^{18}O_{SHELL\_PRED}$ of aragonite based on Figure III-2A.

The predicted shell $\delta^{18}O$ ($\delta^{18}O_{SHELL\_PRED}$) for 2012-2013 appear in Figures III-2B, with

values ranging between -5.9 and 2.4‰. The $\delta^{18}O_{SHELL\_PRED}$ trend appears mostly

temperature-driven in 2012. Values are more irregular in 2013, with declines $\delta^{18}O_{WATER}$

from a January rain storm and higher values in June from increased Lake Whitney flow

proportions. Measured $\delta^{18}O$ and $\delta^{13}C$ values of the ventral margin and INL in each shell

are summarized in Table III-1. Strong overlap in isotopic values is observed for all

ONL-INL transect pairs, regardless of species. Mean $\delta^{13}C$ is consistently lower in the *C.*

tampicoensis specimens than in the *A. plicata* specimens. Figure III-3 plots the oxygen

and carbon isotope results from high-resolution microsamples from shell ventral margins

and INL regions from TAMU for 3R5, 3R3, TP2, and TP3 and low-resolution samples

from JHU for both TP2 and 3R5 (Figures III-3A and III-3G). Dashed grey lines align

interpreted synchronous $\delta^{18}O$ minima in each shell according to the assigned growth

chronologies (see discussion below). The shell growth bands do not show any consistent

relationships with seasonal temperatures or isotope values (Table III-2). The trends in

$\delta^{18}O$ and $\delta^{13}C$ were consistent between the INL and ONL areas in each specimen. Based

on the physical distance between successive microsamples, and the assigned

chronologies described below, we estimated shell extension rates in mm/yr (Figure III-

7).

Clumped isotope temperatures, $\delta^{18}O_{WATER}$ ($\delta^{18}O_{WATER\_\Delta47}$) calculated from

clumped temperatures using Dettman et al. (1999), and σ values are presented in Table

III-1. The 3R5 measurements yield two cool temperatures (21 ± 3 °C and 19 ± 3 °C) and

two warm temperatures, (32 ± 4 °C, 33 ± 3 °C), and $\delta^{18}O_{WATER\_D47}$ values from $-0.4 \pm$

0.7‰ to 1.5 ± 0.6‰. The TP2 clumped isotope temperatures vary from 26 ± 5 °C to 36

according to the assigned growth chronologies (see discussion below). The shell growth

bands do not show any consistent relationships with seasonal temperatures or isotope

values (Table III-2). The trends in $\delta^{18}O$ and $\delta^{13}C$ were consistent between the INL and
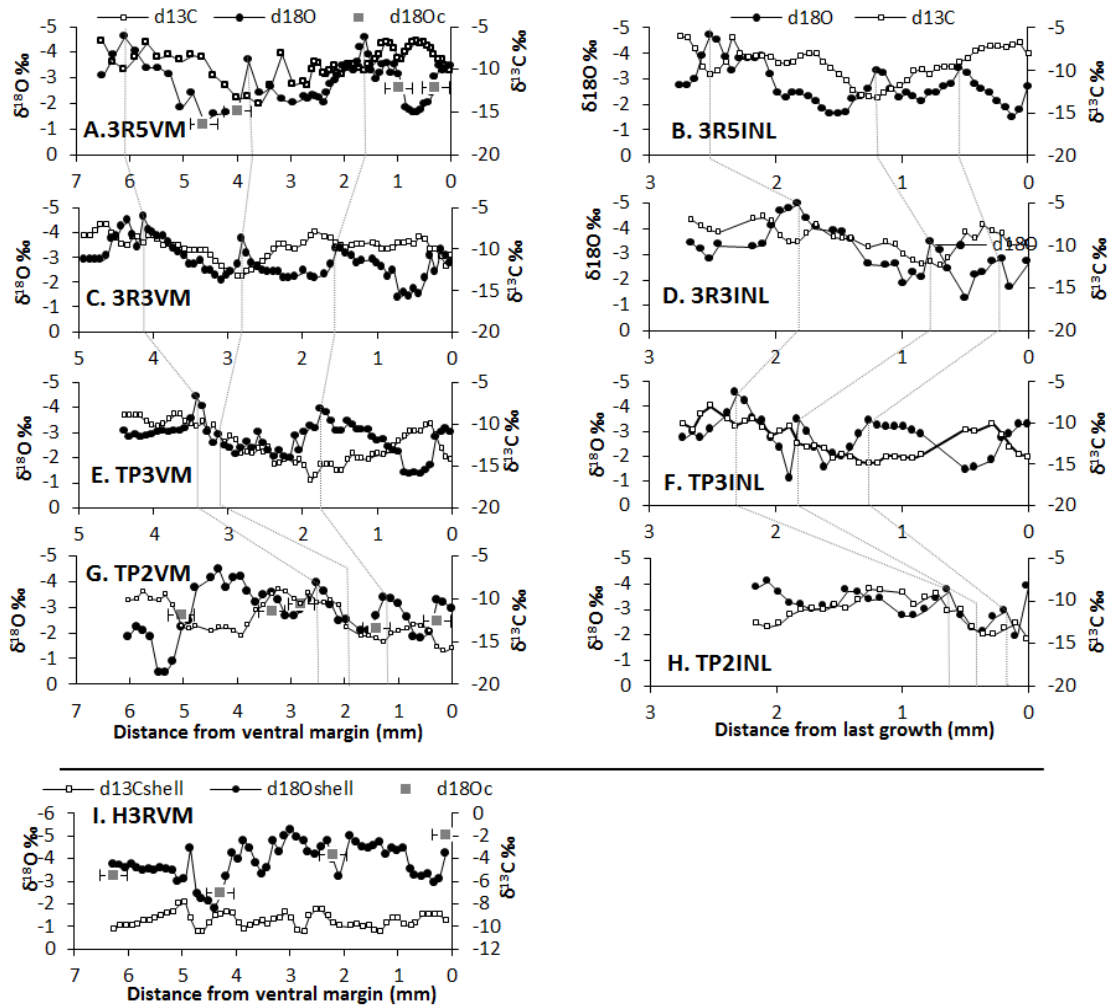
Figure III-3. Mussel shell $\delta^{18}O$ and $\delta^{13}C$ series alignment. Time series $\delta^{18}O$ (black circles) and $\delta^{13}C$ (white squares) data from TAMU for shell transects for 3R5VM (A), 3R5INL (B) , 3R3VM (C), 3R3INL (D), TP3VM (E), TP3INL (F), TP2VM (G), TP3INL (H), and H3RVM (I). The $\delta^{18}O$ from JHU, or"d18Oc" in the legend, are gray squares with error bars in 3R5VM (A) and in TP2VM (G). Gray dotted lines connect cyclical minima in each transect.

41

ONL areas in each specimen. Based on the physical distance between successive microsamples, and the assigned chronologies described below, we estimated shell extension rates in mm/yr (Figure III-7).

Clumped isotope temperatures, $\delta^{18}O_{WATER}$ ($\delta^{18}O_{WATER\_\Delta47}$) calculated from clumped temperatures using Dettman et al. (1999), and σ values are presented in Table III-1. The 3R5 measurements yield two cool temperatures (21 ± 3 ˚C and 19 ± 3 ˚C) and two warm temperatures, (32 ± 4 ˚C, 33 ± 3 ˚C), and $\delta^{18}O_{WATER\_D47}$ values from -0.4 ± 0.7‰ to 1.5 ± 0.6‰. The TP2 clumped isotope temperatures vary from 26 ± 5 ˚C to 36 ± 2 ˚C, while $\delta^{18}O_{WATER\_\Delta47}$ values vary from -1.2 ± 1.2‰ to 0.8 ± 1.1‰. The clumped temperatures at the shell ventral margins are higher than the 30 days preceding the shell collection date by 2.9 ˚C in 3R5 and 4.9 ˚C in TP2. This may indicate a problem with the clumped temperature calibration, as discussed below. The clumped temperatures for the historic Threeridge shell (H3R) (27 ± 2 ˚C to 36 ± 4 ˚C) are similar to those obtained for modern shells, while the $\delta^{18}O_{WATER\_\Delta47}$ range (-2.5 ± 0.4‰ to 0.1 ± 0.6‰) hints at, but because of uncertainty does not confirm, lower values. Figure III-4 plots relationships between Brazos River discharge (Q) and $\delta^{18}O_{WATER}$ at the study site. There is a significant logarithmic relationship for the entire data set ($R^2 = 0.1965$, $r = 0.443$, $p < 0.001$) and for the cooler months of the year (Oct-Apr, $R^2 = 0.2914$, $r = 0.540$, p < 0.001), but not for the warm months of the year (May-Sep, $R^2 = 0.0356$, $r = 0.189$, $p > 0.1$).

TABLE III-1. MUSSEL SHELL δ^{18}O AND δ^{13}C SUMMARY STATISTICS. SHELL CARBON AND OXYGEN ISOTOPE RANGES FOR VENTRAL MARGIN AND INL REGIONS IN 3R5 AND TP2. G IS GROWTH RATE IN MM/YR

		δ^{18}O ‰				δ^{13}C ‰						
		x̄	se	min	max	x̄	se	min	max	N	Ḡ	σ
3R5	VM	-2.8	0.1	-4.6	-1.3	-9.3	0.2	-14.2	-6.7	58	8.2	2.3
	INL	-2.7	0.1	-4.7	-1.5	-9.1	0.3	-13.3	-6.0	48	3.4	1.4
TP2	VM	-2.8	0.1	-4.5	-0.4	-12.2	0.3	-16.6	-8.9	43	3.0	1.8
	INL	-3.2	0.1	-4.1	-2.0	-11.3	0.4	-14.6	-8.7	25	5.8	3.6
3R3	VM	-2.8	0.1	-4.6	-1.4	-9.8	0.2	-13.2	-7.0	57	6.8	1.8
	INL	-3.1	0.2	-5.0	-1.3	-9.2	0.3	-12.4	-6.7	32	1.8	0.6
TP3	VM	-2.7	0.1	-4.4	-1.3	-12.4	-0.3	-16.8	-8.9	62	9.2	4.9
	INL	-2.8	0.1	-4.5	-1.1	-12.1	0.3	-14.9	-7.9	34	4.9	2.0
H3R	VM	-3.8	0.1	-5.3	-1.8	-9.5	0.1	-10.6	-7.9	56		
HTP	VM	-3.2				-11.6				2		

43

TABLE III-2. SHELL CLUMPED ISOTOPE DATA SUMMARY. SAMPLE Δ_{47}, CLUMPED ISOTOPE TEMPERATURE, AND BACKED-OUT $\delta^{18}O_{WATER\_\Delta47}$ AND ASSOCIATED PRECISION RESULTS. TEMPERATURES WERE CALCULATED USING THE PALEOTEMPERATURE EQUATION FROM HENKES ET AL. (2013). THE COLUMN "B" STANDS FOR BANDING, "D" IS DARK, AND "L" IS LIGHT.

Sample	Δ_{47}	σ	T^oC	σ	$\delta^{18}O_{WATER\_D47}$	σ	B
3R5_0.3	0.667	0.006	33	3	-0.4	0.7	D
3R5_0.9	0.668	0.009	32	4	-0.3	0.9	D
3R5_3.9	0.697	0.008	21	3	1.5	0.6	L
3R5_4.6	0.700	0.007	19	3	1.3	0.6	D
TP2_0.3	0.661	0.012	35	5	-1.2	1.2	L
TP2_1.4	0.684	0.012	26	5	0.8	1.1	L
TP2_2.7	0.671	0.001	31	1	0.5	0.1	L
TP2_3.2	0.661	0.005	36	2	-0.8	0.6	L
TP2_4.9	0.678	0.010	28	4	0.8	1.0	D
H3R_0.3	0.659	0.011	36	4	-1.3	1.0	D
H3R_2.0	0.681	0.004	27	2	-2.5	0.4	D
H3R_4.3	0.672	0.007	31	3	0.1	0.6	L
H3R_5.7	0.671	0.009	31	4	-0.6	0.9	D
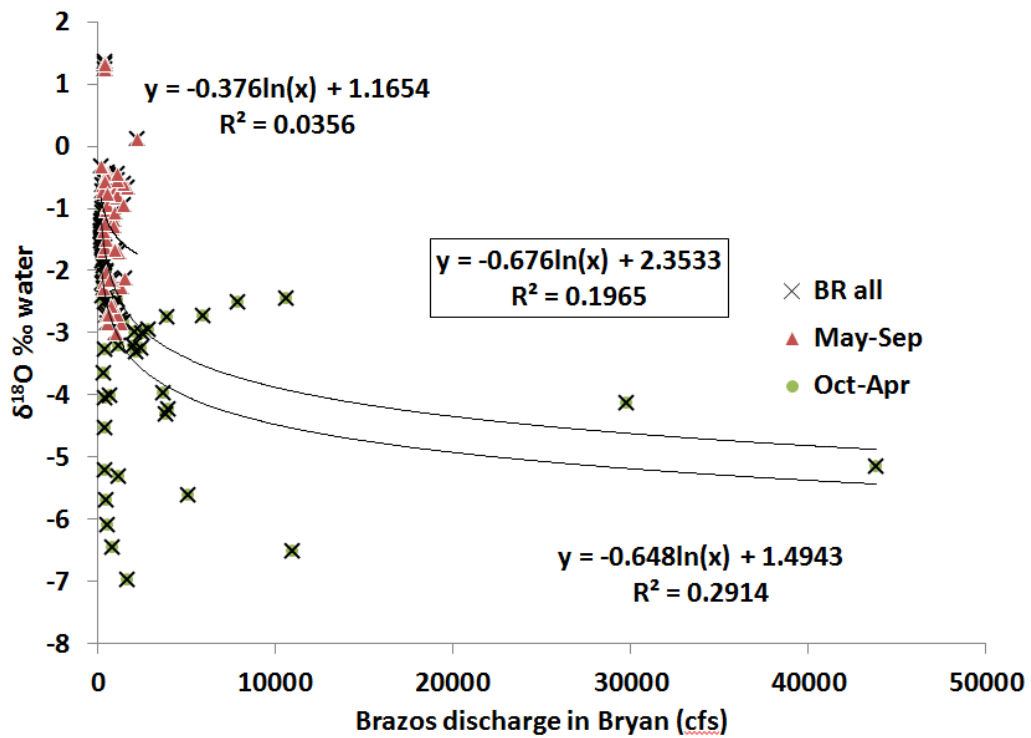
Figure III-4 Brazos River discharge vs. δ^{18}O. Logarithmic correlation between discharge in cubic feet per second (cfs) and water δ^{18}O for 2012-2013 in the Brazos River near Bryan-College Station. All data are in X's and its regression equation is in the center of the plot in a black box, and warm temperature data (May-Sep) are red triangles and that regression equation is at the top of the plot, and cool temperature data (Oct-Apr) are green circles and that regression equation is at the bottom of the plot.

Discussion

Although Δ_{47} temperatures were not used to assign weekly shell growth as with the micromilled $\delta^{18}O$ record, assigning shell growth chronologies began with identifying contrasting warm and cold Δ_{47} temperatures in the 3R5 and TP2, which are presented in Figure III-5 along with $\delta^{18}O_{WATER\_\Delta47}$ estimates that were not used as the primary basis for assigning shell growth chronologies. In 3R5 the contrasting Δ_{47} temperatures dictated how the predicted and observed shell $\delta^{18}O$ time series were aligned, while TP2 lacked distinct cold temperatures suggesting a prolonged growth hiatus through winter in that particular specimen. The low resolution $\delta^{18}O$ value collected with each clumped isotope analysis is anchored to a value in the high resolution micromilled $\delta^{18}O$ data series, as shown in Figure III-3. After determining the growth temperatures for shell increments in 3R5 and TP2, predicted shell $\delta^{18}O$ and micromilled $\delta^{18}O$ values were paired to generate growth chronologies (Figure III-6) with weekly precision that fit the temperature ranges

indicated by Δ_{47} values. The clumped temperature values are on average 4˚C higher than corresponding observed water temperatures. The composite and aragonite-specific equations (for 90˚C acid) from Defliese et al. (2015; equations 4 and 6 therein) produce even higher clumped paleotemperature estimates than the Henkes et al. (2013) bivalve and brachiopod equation used here. Six of the nine $\delta^{18}O_{WATER\_\Delta47}$ estimates fall on the measured water $\delta^{18}O_{WATER}$ series when plotted according to the assigned shell growth chronologies (Figure III-5B).

In order to assign chronologies to specimens 3R3 and TP3 which did not have Δ_{47} temperatures, we identified isotope value cycles across transects as depicted with dashed lines in Figure III-3. $\delta^{13}C$ trends appear to be generally consistent between transects, and INL and VM isotope values show similar trends both between and within shells. However, we did not use $\delta^{13}C$ profiles or direct comparison between INL and VM transects as primary methods for assigning shell growth chronologies, although those methods were used to resolve some ambiguous chronology assignments such as where precisely in the shell record do values appear to jump from autumn to spring, skipping winter, which ultimately involves some arbitrary interpretation. Besides $\delta^{13}C$ profiles and intra-shell comparisons, another candidate for guiding shell $\delta^{18}O$ chronologies is the shell extension rate implied by a proposed chronology. If a chronology implies
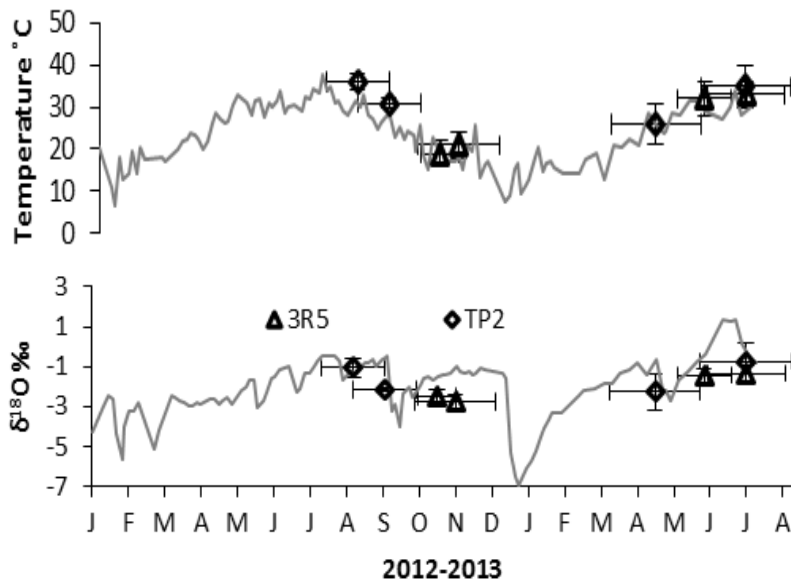
Figure III-5. Clumped isotope temperature and water δ'°O chronologies. Clumped isotope temperatures (A) and $\delta^{18}O_{WATER\_\Delta47}$ (B) chronologies combining 3R5 and TP2 data, based on the $\delta^{18}O_{SHELL}$ chronologies.
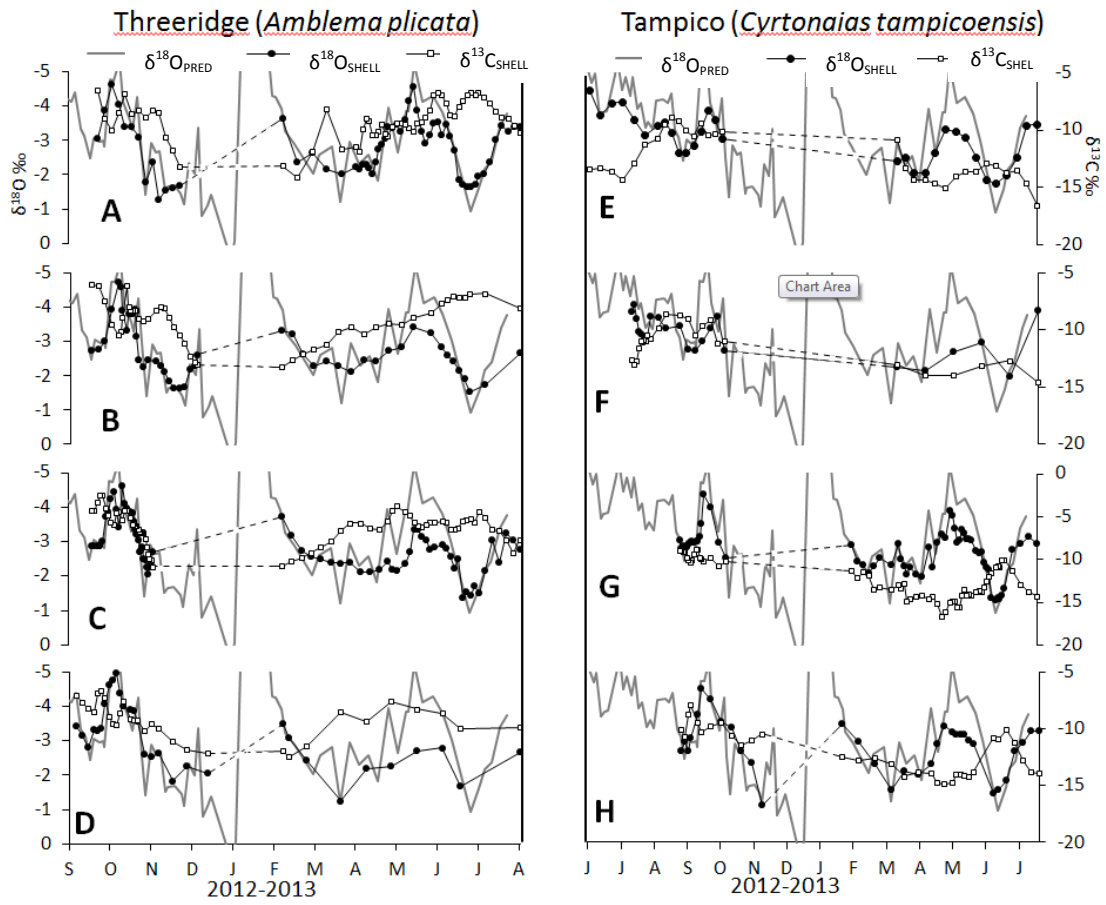
Figure III-6. Shell isotope chronologies. 3R5VM (A), 3R5INL (B), 3R3VM (C), 3R3INL (D), TP2VM (E), TP2INL (F), TP3VM (G), and TP3INL (H).

accelerating growth from one year to the next, particularly in juvenile mussels whose growth rate is expected to resemble exponential decay (Haag and Rypel, 2011), then the chronology deserves extra scrutiny. In this study, growth rate was used as a secondary means of evaluating proposed shell growth chronologies.

Average growth rates for the shells range from assumed winter dormancy (0 mm/yr) to growth spurts of 23 mm/yr, and were not significantly different between species (Figure III-7; $p < 0.05$). The growth rate chronologies indicate that for all four modern shells, the INL growth rate is generally less than the ventral margin (or ONL) growth rate. Figures III-5 show similar winter growth hiatuses between *Amblema plicata* and *Cyrtonaias tampicoensis*. While growth rate itself depends on ontogeny (Haag and Rypel, 2011), there did not appear to be significant differences in the growth rate variability or growth spurt patterns between individuals in this study. Also, this study failed to identify a significant relationship between shell banding pattern and temperature (Table III-2) similar to findings in oyster studies (Surge et al., 2001; Langlet et al., 2006). While I attempted to age the shells by counting their light and dark growth bands (Neves and Moyer, 1988), inconsistency in shell banding casts doubt on applying this method here. Because I consistently inferred winter growth hiatuses in these species (*A. plicata* vs. *C. tampicoensis*), this study highlights the potential for 1) variable shell growth rate, and 2) gaps in shell records from growth cessation. While mark-recapture studies produce empirical shell growth rates (Goewert et al., 2007; Haag and Commens-Carson, 2008; Haag, 2009), combining clumped isotope temperatures and micromilled oxygen isotope chronologies may provide more detailed information on shell growth.

Carbon isotope values are consistently significantly lower in *Cyrtonaias tampicoensis* than *Amblema plicata*. Because metabolic carbon has lower $\delta^{13}C$ values, this may be evidence of differences in the rate of incorporation of metabolic carbon in shells between the two species (McConnaughey and Gillikin, 2008). Shell carbon isotope data aid in matching $\delta^{18}O$ chronologies without knowing water DIC $\delta^{13}C$ thanks to consistent trends in $\delta^{13}C$ in the shell INL and ONL regions (Figure III-5 and III-6). In Elliot et al. (2009) and Ivany et al. (2004), $\delta^{18}O$ and $\delta^{13}C$ ranges were similar between inner and outer laminated accretionary regions in the bivalves studied, although they did not observe similar trends in values between regions within shells. Based on the assigned growth chronologies in this study, $\delta^{13}C$ trends appear to track one another between the inner and outer nacreous shell regions. The observed $\delta^{13}C$ increases in summer in both species studied appear to reflect seasonal phenomena, possibly environmental DIC availability, mussel metabolic activity, or a combination of the two. The positive shifts in shell $\delta^{13}C$ summer values may represent the influence of relatively high $\delta^{13}C$ (~-6‰) Lake Whitney water (Zeng et al., 2011) dominating flow in the summer in 2012-2013, particularly during the Texas drought (CHAPTER II). We hypothesize that relatively high baseline $\delta^{13}C$ values (-10 to -6‰) seen in summer growth from 2012-13 alternate with low $\delta^{13}C$ (-18 to -11‰) values seen in winter, spring, and fall, but more water $\delta^{13}C_{DIC}$ data are needed to test this.

I compared observed Brazos River discharge near College Station with discharge estimated from the observed $\delta^{18}O_{WATER}$, from $\delta^{18}O_{WATER\_D47}$, or from calculated
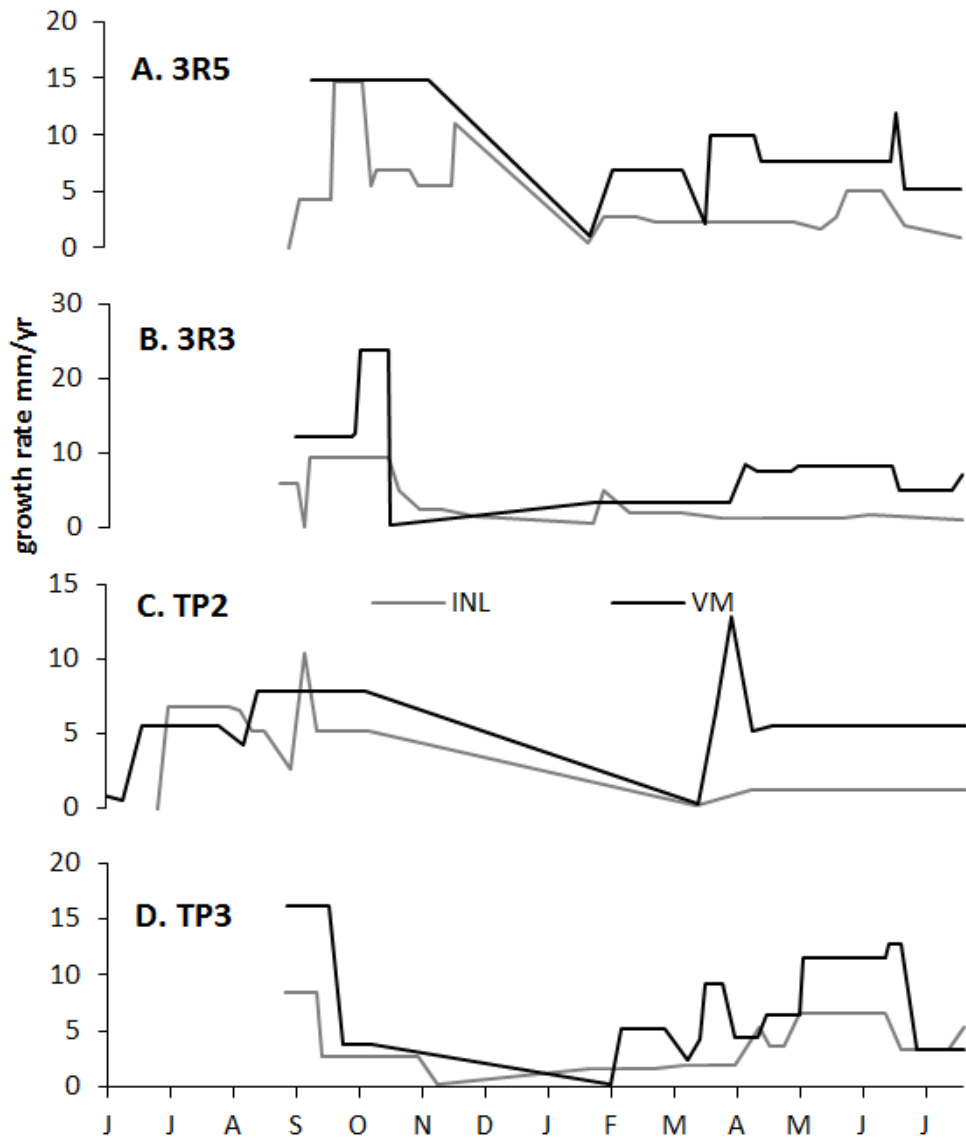
Figure III-7. Shell growth rate chronologies. Growth rate (mm/yr) for 3R5 (A), 3R3 (B), TP2 (C), and TP3 (D), where the gray line is INL growth rate and the black line is VM growth rate.

$\delta^{18}O_{WATER}$ based on observed $\delta^{18}O_{SHELL}$ in 3R5 and water temperature data using the sinusoidal equation:

$$T \ (°C) = 9 * COS(date/56.88) + 23 \qquad\qquad (III\text{-}5)$$

where date is days after 1900 as in Microsoft Excel (version 2010). The three reconstructed discharge curves relied on the regression equation between Brazos River discharge and $\delta^{18}O_{WATER}$ for all samples (BR all) from 2012-2013 (Figure III-3). The more deterministic relationship between $\delta^{18}O_{WATER}$ and discharge Q for all Brazos River measurements ($r = 0.\ 443$) and for October-April ($r = 0.540$) than for May-September ($r = 0.189$) indicates that $\delta^{18}O_{WATER}$ reconstructs Brazos River discharge (Q) more accurately for cool intervals than for the warm ones, in contrast to Versteegh et al. (2010b). This is because the Brazos is subject to strong influence from reservoir flow in the summer and storm runoff in the winter, in contrast to the winter dominance of groundwater in the River Meuse in Versteegh et al. (2010b). Besides using modeled temperature to reconstruct $\delta^{18}O_{WATER}$, clumped isotope estimates of $\delta^{18}O_{WATER}$ can also be used to estimate river discharge based on the observed Q vs. $\delta^{18}O_{WATER}$ relationship.

In Figure III-8, the maximum flow event in 2013 (January, 1,850,000 cfs) can be identified using this method ($\pm$ 24 days). While Brazos River discharge has not been accurately quantified based on the shell isotope data, this method does accurately reconstruct discharge variation based on significant linear covariance between observed discharge and discharge reconstructed from $\delta^{18}O_{SHELL}$ ($r = 0.322$, $p < 0.05$). Also, identifying maximum flow events can make shell-growth chemistry records valuable

tools for reconstructing past flow patterns (Dettman et al., 2004; Stamm and Wingard, 2004; Versteegh et al., 2010b). Sources of inaccuracy may include assigned shell growth chronology and shell and water isotope analytical precision.

Besides discharge, salinity measured as EC, and water source as percentage of Lake Whitney water in Brazos River Q in College Station (%LW; see CHAPTER II) can also be reconstructed. There are consistent significant relationships between shell carbon isotope values and EC and %LW, as shown in Table III-3. Brazos River EC and %LW variability were successfully reconstructed ($p < 0.05$) using TP3VM δ^{13}C data (Figure III-9). This supports using mussel shells for reconstructing a variety of environmental parameters.

This study coincided with the Texas drought that began in 2011 and persisted through 2014. This could have affected the results in some ways, such as through low runoff or high dam release rates affecting river flow components and $\delta^{18}O_{WATER}$. Without the influence of impounded water with high $\delta^{18}O$, the $\delta^{18}O_{SHELL}$ shell values in the Brazos River prior to dam construction were likely more temperature-driven than the modern shell $\delta^{18}O$ values, but higher resolution clumped isotope data are needed to test this hypothesis. While more data are required, the H3R $\delta^{18}O_{SHELL}$ cycles may reflect seasonal temperature cycles (Figure III-4). T-tests indicate that H3R $\delta^{18}O$ was significantly different from all modern shells studied ($p < 0.05$), but HTP $\delta^{18}O$ was not. More shells should be analyzed to determine if the lower $\delta^{18}O$ values in the H3R is

Observed and reconstructed discharge in the Brazos River near Bryan-College Station for 2012-2013
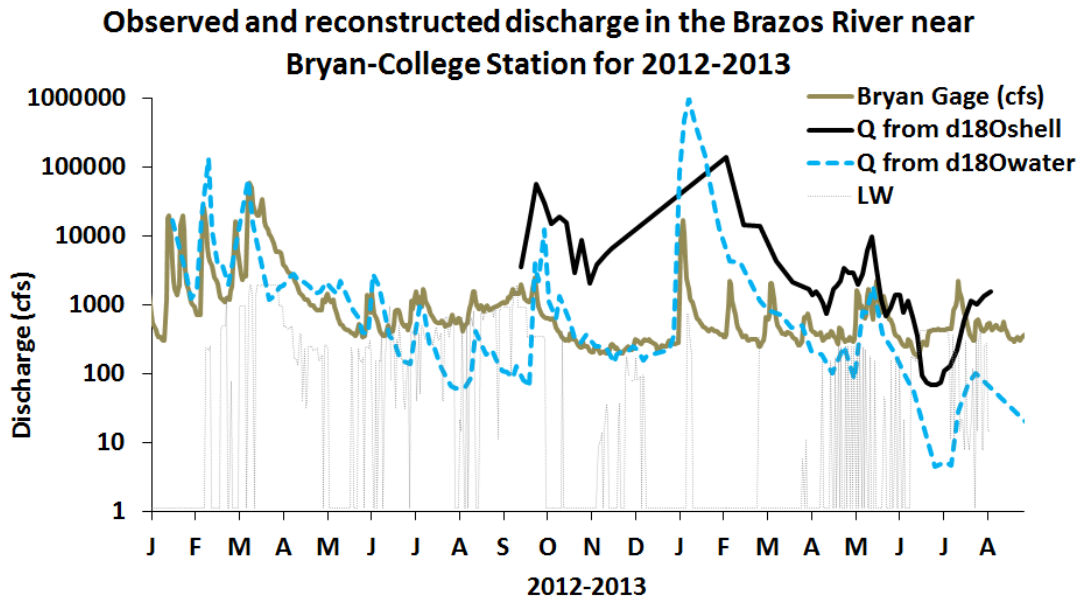
Figure III-8. Brazos River discharge reconstructed from shell $\delta^{18}O$. Observed discharge (brown solid) in the Brazos River near Bryan-College Station; and discharge reconstructed based on water $\delta^{18}O$ measurements (blue dashed); discharge reconstructed from shell $\delta^{18}O$ measurements (black solid) from 3R5 and reconstructed temperature. All reconstructed discharge curves used the regression equation for "BR all" from Figure III-4. There is significant linear covariance between observed discharge and discharge reconstructed from $\delta^{18}O_{SHELL}$ ($r = 0.322$, $p < 0.05$).

TABLE III-3. SHELL CHEMISTRY, WATER SOURCE AND SALINITY COVARIANCE
STATISTICS. PEARSON'S r VALUES FOR δ^{18}O AND δ^{13}C VS. LAKE WHITNEY
CONTRIBUTION TO BRAZOS RIVER DISCHARGE IN BRYAN (%LW), AND ELECTRICAL
CONDUCTIVITY (EC); SIGNIFICANT VALUES ($p < 0.05$) IN BOLD

		%LW	EC	n
3R5VM	δ^{18}O	0.16	**0.29**	56
	δ^{13}C	**0.42**	**0.42**	56
3R5INL	δ^{18}O	0.08	0.32	45
	δ^{13}C	**0.34**	**0.40**	45
3R3VM	δ^{18}O	0.26	0.10	66
	δ^{13}C	**0.46**	**0.28**	66
3R3INL	δ^{18}O	-0.16	-0.25	29
	δ^{13}C	**0.56**	**0.43**	29
TP2VM	δ^{18}O	-0.12	-0.01	33
	δ^{13}C	0.07	**0.43**	33
TP2INL	δ^{18}O	-0.08	0.01	22
	δ^{13}C	**0.48**	**0.47**	22
TP3VM	δ^{18}O	**0.42**	0.21	59
	δ^{13}C	**0.51**	**0.76**	59
TP3INL	δ^{18}O	0.22	0.20	32
	δ^{13}C	**0.39**	**0.71**	32

A. Observed and reconstructed %LW

B. Observed and reconstructed EC
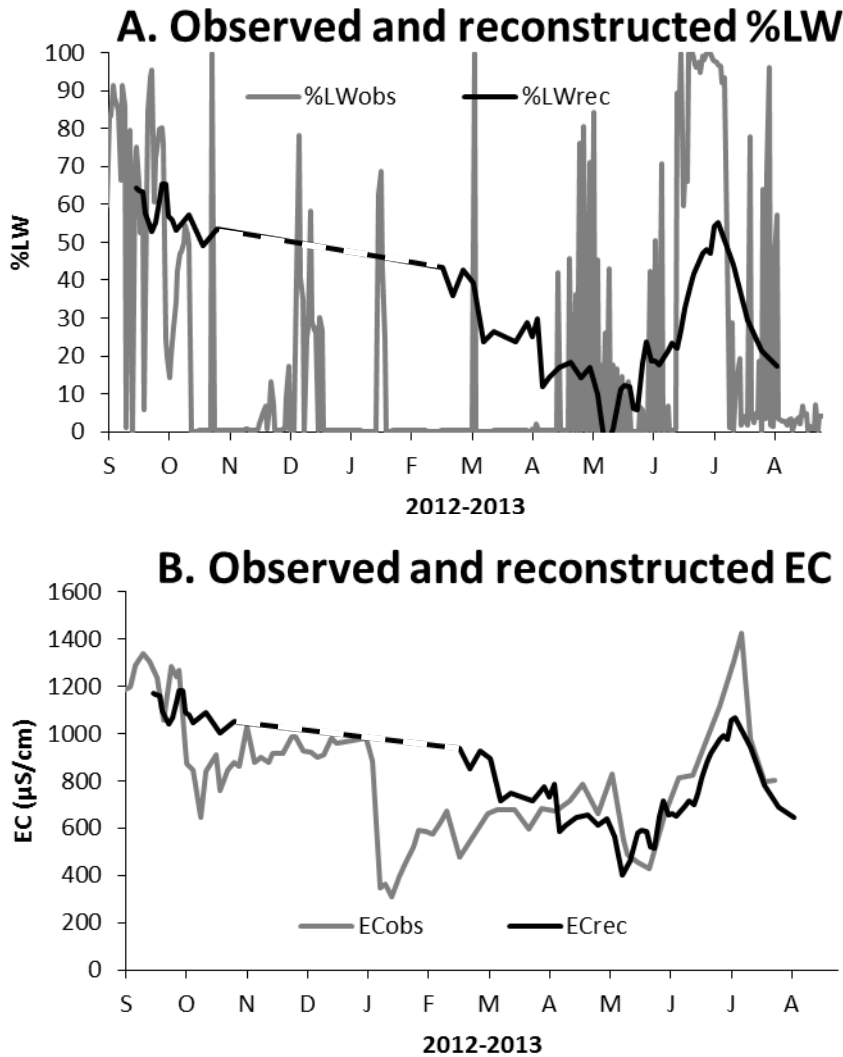
Figure III-9. Reconstructed reservoir release and salinity chronologies. Observed water source as percent of Lake Whitney discharge in the Brazos River in Bryan (%LWobs) represented as a grey line, and reconstructed water source (%LWrec) from TP3 carbon isotopes, where %LW = $9 * \delta^{13}C + 145$, as a black line with the winter hiatus dashed (A), and Pearson's r between reconstructed and observed values was 0.51 ($p < 0.05$). Observed electrical conductivity in the Brazos River (ECobs) represented as a grey line, and electrical conductivity reconstructed from TP3 carbon isotopes as a black line (ECrec), where ECrec = $\delta^{13}C * 99 + 2065$ with the winter hiatus dashed and where $r = 0.71$ between reconstructed and observed EC values and $p < 0.05$ (B).

evidence for more negative average water $\delta^{18}O$ values in a time before major dams, water impoundment, perhaps with less influence of evaporation on river flows.

T-tests indicate *C. tampicoensis* $\delta^{13}C$ values are consistently significantly lighter than *A. plicata* $\delta^{13}C$ values ($p < 0.05$). Lack of a contrast between modern and historical mussel $\delta^{13}C$ values is puzzling because, on the one hand, mollusk $\delta^{13}C$ is known to record the progressive historical decrease in atmospheric $\delta^{13}C$ values from anthropogenic CO_2 emissions (Gentry et al., 2008) termed the Seuss effect where DIC $\delta^{13}C$ ($\delta^{13}C_{DIC}$) values between1970 and 2000 decreased by 0.014-0.018‰ per year (Böhm et al., 1996; Quay et al., 2003). On the other hand, Brazos River $\delta^{13}C_{DIC}$ is believed to have increased as a consequence of on-channel dam construction and formation of reservoirs, which enhances atmospheric exchange and increases $\delta^{13}C$ signal, thereby mitigating the more negative respiration-derived $\delta^{13}C$ signal (Zeng et al., 2011). The Seuss effect and the Brazos River dams probably had opposing effects on river $\delta^{13}C_{DIC}$, which may explain the similar $\delta^{13}C$ values between the historical and modern shells. However, because the historical shells were from older, sexually mature individuals, ontogenetic differences between the sub-adult modern shells and the historical shells may complicate or invalidate our comparison.

Conclusions

The $\delta^{18}O_{SHELL}$ from all four modern specimens show similar values and trends with shell growth and in intra-shell comparisons between the inner nacreous and outer

nacreous regions regardless of species. This indicates that $\delta^{18}O_{SHELL}$ is a valid chronometer, although the inner nacreous layer did not capture as much of the extreme $\delta^{18}O$ values as the ventral margin. We observed consistent intra-shell and inter-shell $\delta^{13}C$ trends. This may be evidence upstream dam releases from Lake Whitney strongly influencing $\delta^{13}C_{DIC}$. Clumped isotope temperatures of shell growth layers can be used to determine the seasons in which shell segments grew. The use of clumped isotopes as corroborating evidence improves the accuracy of sclerochronology in an environmental study where $\delta^{18}O_{SHELL}$ records are too difficult to interpret alone due to 1) opposing action of temperature and $\delta^{18}O$ of the water on shell records, and 2) variable shell growth rate. Growth chronologies indicate similar growth patterns and winter growth hiatuses between species. While shell isotope values cannot be used to quantify discharge, $\delta^{18}O_{SHELL}$ can still be used to reconstruct discharge variability and to identify major flow events, as well as to reconstruct salinity and water source variability, indicating that mussel shells can be useful for paleoenvironment reconstruction. The historical Threeridge shell (*A. plicata*) collected prior to Brazos River dam construction may reflect temperature-driven $\delta^{18}O_{SHELL}$ cycles, but higher resolution clumped isotope measurements should be taken to test this. More historical specimens are needed to test whether the lower $\delta^{18}O_{SHELL}$ values in the 100-year-old Threeridge specimen (H3R) than in the modern shells indicate lower $\delta^{18}O_{WATER}$ values in the Brazos River before dams were constructed. Identical $\delta^{13}C$ values between historical and modern shells indicates that the opposing actions of dam construction and anthropogenic CO_2. Carbon isotope values are consistently significantly lower in *Cyrtonaias tampicoensis* than *Amblema*

plicata. This may be evidence of differences in the rate of incorporation of metabolic

carbon in shells between the two species.

CHAPTER IV

TRACE ELEMENTS IN FRESHWATER MUSSEL SHELLS FROM THE BRAZOS

RIVER IN TEXAS: ENVIRONMENTAL VERSUS BIOLOGICAL CONTROLS

Introduction

Determining the environmental and biological controls on mollusk shell trace

element composition is crucial for 1) using shells as environmental recorders and 2)

understanding mollusk life cycles and adaptations, and 3) applying this information to

the geological record. Stable isotope records in mussel shells are important

environmental archives, serving to record temperature, river discharge, and water source

(Dettman et al., 1999; Dettman et al., 2004; Versteegh et al., 2010a; Versteegh et al.,

2010b). Shell Ba/Ca and Mn/Ca values are often correlated with bioproductivity

(Stecher et al., 1996; Vander Putten et al., 2000; Lazareth et al., 2003). However, it has

been widely observed that mollusk metabolic rate controls shell Sr/Ca, and metabolism

is in turn controlled by many variables such as water temperature, food availability,

sexual maturity, and reproductive activity (Gillikin et al., 2005; Carré et al., 2006;

Gentry et al., 2008; Izumida et al., 2011). Similarly, a study of cathodoluminescence in

oysters suggested a relationship between temperature, metabolic rate and shell Mn/Ca

(Langlet et al., 2006). While partly calcitic bivalve shell Mg/Ca has shown positive

correlation with seawater temperature (Dodd, 1967; Klein et al., 1996; Lazareth et al.,

2003), such correlation is absent in some shells from brackish and freshwater environments (Vander Putten et al., 2000; Izumida et al., 2011).

Imperiled by dams, river diversions, and intensive farming (Richter et al., 1997), freshwater mollusks are in decline world-wide, prompting calls for conservation (Lydeard et al., 2004) and increased environmental and ecological research order to implement better conservation strategies (Strayer et al., 2004). This is an issue in the Brazos River watershed in Texas (Randklev et al., 2013), where dams on the main channel and tributaries influence stream ecology by altering river flow, water temperature, salinity, and host fish migration ranges. Other risks to Texas mussels include bank deforestation and cattle encroachment.

We studied a specimen each of *Amblema plicata* and *Cyrtonaias tampicoensis*, common freshwater mussel species, collected from the Brazos River in College Station, Texas in 2013. Shells were analyzed by paired stable isotope and trace element analyses (Mn, Sr, Ba, Ca, Mg) using isotope ratio mass spectrometery (IRMS) and solution-based high resolution inductively-coupled-plasma mass spectrometry (HR-ICP-MS) respectively. In each shell the ventral margin (VM) and inner nacreous layer (INL) areas were micromilled to examine high-resolution (weekly) trace element and carbon and oxygen isotope variability throughout coeval growth intervals within and between shells. From our previous study, oxygen and clumped isotope data were used to assign shell growth intervals to a high resolution chronology (CHAPTER III), and this formed the basis for investigating seasonal variability in trace element concentrations in the shells.

Mn/Ca results were compared with cathodoluminescence images to demonstrate the high spatial resolution of micromilling coupled with solution-based HR-ICP-MS measurements. Cathodoluminescence also demonstrated that Mn largely accumulated in the mineral lattice rather than the organic proteinaceous shell matrix.

Methods

This study focuses on the middle run of the Brazos River near College Station, Texas about 210 km north of Freeport, where the Brazos flows into the Gulf of Mexico (Figure II-1). The Brazos flows southeast through a semi-arid to semi-humid climate characterized by hot summers and mild winters, averaging 29˚C and 13˚C, respectively (Nielsen-Gammon, 2012). Average annual rainfall in College Station is 100 cm, flashy, and historically peaks in late-spring and mid-fall. About 240 km upstream of the study site is Lake Whitney, dammed for hydropower and flood control. About 30 km upstream of the study site is the confluence with the Little River, the largest Brazos tributary, receiving flows from Lake Belton, Stillhouse Hollow Lake, and Granger Lake, all dammed reservoirs.

From January 2012 through July 2013, weekly temperature measurements and water $\delta^{18}O$ samples were collected from the Brazos River at the Highway 60 bridge between Brazos and Burleson counties. Water samples were measured for $\delta^{18}O$ and δD using a Picarro L2120i cavity ringdown spectrometer at the Stable Isotope Geoscience Facility at Texas A&M University (TAMU) with calibrations detailed in CHAPTER II.

Brazos River discharge data from the gage at Highway 21 near College Station (USGS 08108700) were obtained online from http://waterdata.usgs.gov/tx. Water $\delta^{18}O$ and temperature are discussed in detail in CHAPTER II and summarized here. $\delta^{18}O$ ranges from -7.0 to 1.4‰, and temperature ranges from 6.7 to 37.8 ˚C (Figure IV-2). Temperature and $\delta^{18}O$ covary strongly but not highly deterministically ($r^2 = 0.28$, $N = 120$, $p < 0.05$). Increased evaporation combined with increased release of evaporated ^{18}O-enriched Lake Whitney water lead to intermittently high $\delta^{18}O$ in the summer, whereas ^{18}O-depleted precipitation and runoff lead to lower $\delta^{18}O$ in the winter (Chowdhury et al., 2010; CHAPTER II). These temperature (T) and water $\delta^{18}O$ ($\delta^{18}O_{WATER}$ in ‰ VSMOW) measurements, along with the aragonite oxygen isotope thermometry equation from Dettman et al. (1999; based on Grossman and Ku, 1986), were used to predict shell $\delta^{18}O$ according to equations III-1, III-2, and III-3. On August 9, 2013, four specimens each of *Amblema plicata* and *Cyrtonaias tampicoensis* were collected live from the Brazos River near the Highway 60 bridge, from the sandy river bed shallower than 2 m depth. Mussels were frozen, then shucked. Shells were scrubbed, sonicated in water, and dried.

One specimen each of modern young adult *A. plicata* (labelled 3R5) and *C. tampicoensis* (TP3) were analyzed. Based on age estimation techniques from Neves and Moyer (1988), counting light and dark bands, mussel ages upon death were approximately 3-7 years old. Specimens were sectioned, broken in two, and epoxied to glass slides (Figures IV-3A and IV-3B). Shell powder samples were collected with a New Wave micromill using a 0.5 mm drill bit following the methods of Dettman and

Lohmann (1995). In each shell two transects were sampled: one across the ventral margin region (or VM, sometimes referred to as the outer nacreous layer or ONL), and one across the INL region (inner nacreous layer, or INL; Figure IV-3). Sample intervals were between 60 and 140 µm, with generally shorter spacing for INL than ONL. About 60 µg per sample were reacted in a Kiel IV carbonate instrument with "100%" orthophosphoric acid and the CO_2 analyzed on a Thermo Finnigan MAT253 mass spectrometer at Texas A&M University (TAMU). Average analytical precision was 0.05‰ for $\delta^{18}O$ and 0.03‰ for $\delta^{13}C$.

For ICP-MS analysis, 20-160 µg of powder were dissolved in 2 mL of 2% nitric acid solution. ICP-MS was performed on a Thermo Scientific, high resolution inductively-coupled plasma mass spectrometer (HR-ICP-MS) at Texas A&M University's Williams Radiogenic Isotope Geosciences Laboratory for the following nuclides: ^{25}Mg, ^{43}Ca, ^{55}Mn, ^{88}Sr, and ^{137}Ba. The USGS MACS3 coral reference standard was used as a working standard, and 0.2 mL of indium was added to all samples and standards to monitor instrumental drift. Standard error for ratios of metal to calcium < 10%. Also, monthly water Brazos River samples from 2012-2013 were analyzed at the Texas A&M University Soil Water Forage Testing Laboratory for Ca^{2+} and Mg^{2+} using ICP-MS.

Specimens were photographed with cathodoluminescence microscopy (CL) using a Technosyn 8200 MKII cold cathode luminoscope, following the methods of Roark et al. (in press). Samples were exposed to a beam current and voltage of 400 nA and 20 kV,

respectively, for 4-45 s. Using ImageJ software, brightness profiles were plotted from the same locations in the shells as the micro-drilled transects. While some photographs had shadows in the bottom left corners, shadows were cropped out in the INL regions. In order to avoid shadows in the VM regions, ImageJ transects were angled above the bottom left corners of photographs. Image brightness profiles were linearly detrended to reduce the effect of long-term drift in the luminoscope and were then compared with ICP-MS results using Pearson's *r* values.

Results

Trace element results are presented in Figure IV-1 along with oxygen and carbon isotope profiles from all four transects. The INL transect data are scaled to align synchronous growth between the two shell regions, using chronologies from CHAPTER III. The INL grows more slowly and has lower time resolution than the VM. In both shells, Sr/Ca and Mn/Ca values are greater in the INL region than in the VM for coeval growth intervals, whereas average Mg/Ca is greater in the VM than in the INL in 3R5. For the 3R5 data, the peaks in Sr/Ca, Mn/Ca, and Ba/Ca values occur in late spring (AMJ) through summer (JAS) and fall (OND), with minima in the winter (JFM), according to the oxygen isotope chronology from CHAPTER III, while TP3 does not display clear seasonal cyclicity in or across trace metal data. Peak trace metal concentrations in 3R5INL only correlate with chronology-inferred water temperature for
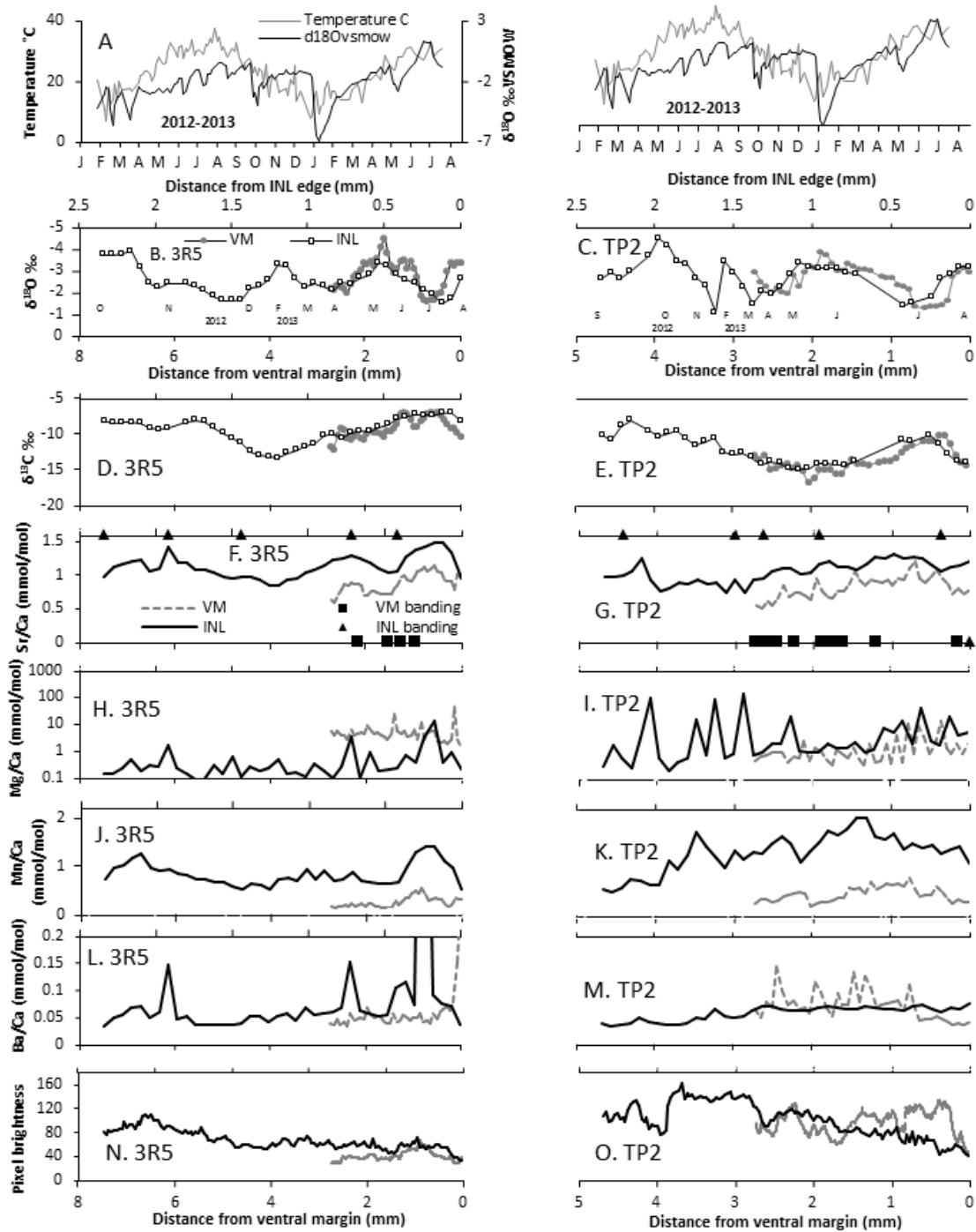
Figure IV-1. Shell trace element data with shell length. Brazos River water temperature and $\delta^{18}O$ values for 2012-2013 (A), 3R5 $\delta^{18}O$, $\delta^{13}C$, Sr/Ca, Mg/Ca, Mn/Ca, and Ba/Ca, and raw CL results (B, D, F, H, J, L and N, respectively), and TP3 $\delta^{18}O$, $\delta^{13}C$, Sr/Ca, Mg/Ca, Mn/Ca, and Ba/Ca, and raw CL results (C, E, G, I, K, M and O, respectively). 2B and 2C include month labels from the isotope chronologies.

Sr/Ca, but not for Mn/Ca, Ba/Ca, or Mg/Ca (Table 1). Therefore there must be significant offset between Sr/Ca and Mn/Ca cycles in 3R5, or there is some error ($\pm$ 1month for the winter hiatus isotope values; see CHAPTER III) in the shell growth chronologies.

Table IV-1 gives standard linear regression Pearson's r values for the linear covariance between the trace elements and stable isotopes in INL and VM transects in 3R5 and TP3. Crossplots comparing Sr/Ca, Mn/Ca, $\delta^{13}C$, %LW, and Ba/Ca are presented in APPENDIX A. Sr/Ca and Mn/Ca correlate significantly ($p < 0.05$) in all transects. Sr/Ca and $\delta^{13}C$ have significant relationships in all transects except in TP3 INL. Mn/Ca and $\delta^{13}C$ correlate positively in both 3R5 transects and negatively in TP3INL. Ba/Ca and Mn/Ca significantly covary in both INL transects but not the VM transects. Mg/Ca and Mn/Ca have significant relationships in both of the VM transects but not in either INL transect, while Ba/Ca and $\delta^{13}C$ have significant negative relationships in both TP3 transects but not in 3R5. Shell $\delta^{18}O$ and Sr/Ca had significant relationships in both VM transects but not in the INL transects.

In Table IV-1, r values are also provided for the relationships between shell trace element concentrations and the river temperature, electrical conductivity (EC, in $\mu S/cm$), percent of discharge through the study site comprised of Lake Whitney outflow (%LW), and daily Brazos River discharge (Q) through College Station for assigned shell growth dates from CHAPTERS II and III. Lake Whitney has > 900 TDS (Wurbs and Lee, 2009), and is regarded as a high salinity endmember in this study. From our previous

TABLE IV-1. SHELL TRACE ELEMENT COVARIANCE STATISTICS. PEARSON'S *R* VALUES FOR RELATIONSHIPS BETWEEN TRACE ELEMENT CONCENTRATIONS AND STABLE ISOTOPE VALUES IN SERIALLY SAMPLED SHELL REGIONS, "H" FOR HINGE AND "V" FOR VENTRAL MARGIN, IN 3R5 AND TP3. N = 40 FOR ALL DATA SETS. G IS SHELL EXTENSION RATE

		Mg/Ca	Mn/Ca	Ba/Ca	$\delta^{13}C$	$\delta^{18}O$	T °C	G	EC (μS)	%LW	Q (cfs)	Inter-shell	CL
3R5 (INL)	Sr/Ca	**0.477**	**0.755**	**0.391**	**0.681**	0.188	**0.430**	-0.021	0.228	**0.357**	0.024	**0.574**	
	Mg/Ca		**0.507**	0.273	0.247	0.204	0.251	-0.077	0.033	**0.498**	-0.018	0.005	
	Mn/Ca			**0.457**	**0.556**	-0.047	0.273	0.324	0.168	0.315	-0.129	-0.113	**0.641**
	Ba/Ca				0.236	0.107	0.235	-0.057	0.002	0.289	-0.080	0.080	
	$\delta^{13}C$					-0.002	**0.645**	0.228	0.306	0.243	-0.008	0.182	
	$\delta^{18}O$						-0.051	**-0.403**	**0.447**	**0.391**	-0.290	**0.631**	
	T °C							-0.045	0.213	**0.467**	0.101	**0.901**	
	G								0.282	-0.131	-0.181	-0.192	
3R5 (VM)	Sr/Ca	-0.129	**0.739**	0.172	**0.776**	**0.460**	0.109	-0.137	**0.513**	0.055	-0.309	0.090	
	Mg/Ca		0.217	0.015	-0.010	-0.050	0.146	-0.258	0.090	-0.079	-0.063	**0.380**	
	Mn/Ca			0.196	**0.559**	0.262	-0.061	-0.083	0.309	-0.323	-0.108	-0.034	**0.605**
	Ba/Ca				-0.118	-0.193	0.063	-0.195	0.219	-0.016	0.143	-0.222	
	$\delta^{13}C$					0.269	**0.614**	-0.088	**0.455**	**0.449**	-0.137	**0.726**	
	$\delta^{18}O$						-0.203	0.181	**0.530**	**0.499**	-0.351	**0.884**	
	T °C							**-0.500**	0.255	0.174	-0.009	**0.939**	
	G								-0.173	0.059	-0.253	0.247	
TP3INL	Sr/Ca	-0.292	**0.440**	**0.645**	-0.331	0.288	**0.738**	0.387	-0.014	**0.410**	-0.078		
	Mg/Ca		-0.148	-0.046	0.122	0.185	-0.210	-0.168	0.129	-0.047	-0.059		
	Mn/Ca			**0.713**	**-0.623**	0.286	0.182	-0.212	**-0.506**	-0.234	**-0.610**		**0.395**
	Ba/Ca				**-0.743**	0.437	0.361	-0.119	**-0.379**	-0.073	**-0.423**		
	$\delta^{13}C$					-0.019	-0.189	0.154	**0.709**	**0.389**	**0.360**		
	$\delta^{18}O$						-0.125	-0.138	0.196	0.215	**-0.421**		
	T °C							**0.619**	0.199	**0.447**	0.224		
	G								-0.014	**0.410**	-0.078		
TP3VM	Sr/Ca	0.371	**0.690**	0.174	**0.444**	**0.352**	**0.488**	**0.490**	0.215	**0.576**	-0.299		
	Mg/Ca		0.266	-0.097	**0.429**	**0.340**	0.077	0.228	0.298	**0.452**	-0.171		
	Mn/Ca			0.249	0.296	0.256	**0.377**	**0.544**	0.095	**0.361**	**-0.560**		
	Ba/Ca				**-0.402**	-0.248	-0.182	0.172	**-0.542**	-0.287	-0.098		**0.461**
	$\delta^{13}C$					**0.724**	0.193	0.311	**0.777**	**0.711**	-0.341		
	$\delta^{18}O$						-0.228	0.275	**0.667**	**0.670**	**-0.468**		
	T °C							0.186	0.213	0.229	-0.010		
	G								0.007	**0.376**	-0.054		

study, %LW tends to be highest in the summer due to low runoff conditions and high Lake Whitney discharge for hydropower, and EC generally tracks %LW, while Q is generally lower in the summer and higher in fall, winter, and spring. Temperature correlates with shell $\delta^{13}C$ in 3R5 but not in TP3, and EC and %LW positively correlate with $\delta^{13}C$ in all shell regions except 3R5INL, but shell $\delta^{18}O$ negatively correlates with Q in all shell regions except for 3R5INL. Also, EC and shell $\delta^{18}O$ positively correlate in all shell regions except TP3INL. Sr/Ca has significant relationships with %LW in all transects except 3R5VM. TP3 growth rate in both the INL and VM transects correlated with both Sr/Ca and with %LW, but this was not observed in 3R5.

Inter-shell correlations in Table IV-1 are based on assigned growth chronologies from CHPTER III. Because the dates of the microsamples were not identical, measured values dated at five days apart or less were compared between 3R5 and TP3. Only shell $\delta^{18}O$, and chronology-inferred water temperature correlated between shells consistently in comparing both the INL and VM regions. Sr/Ca correlated between the INL regions, while Mg/Ca and $\delta^{13}C$ correlated between the VM regions.

Photomosaics of cathodoluminescence (CL) images superimposed on optical scans of the shell cross-sections are presented in Figure IV-2. The CL images show bright and dim yellow-green banding patterns that are in the same orientation, but do not show the exact same light/dark pattern, as the light and dark banding in the optical scans, consistent with observations summarized in Barbin (2000) and a study of oysters by Langlet et al. (2006). The raw CL data (not detrended) from the different shell regions
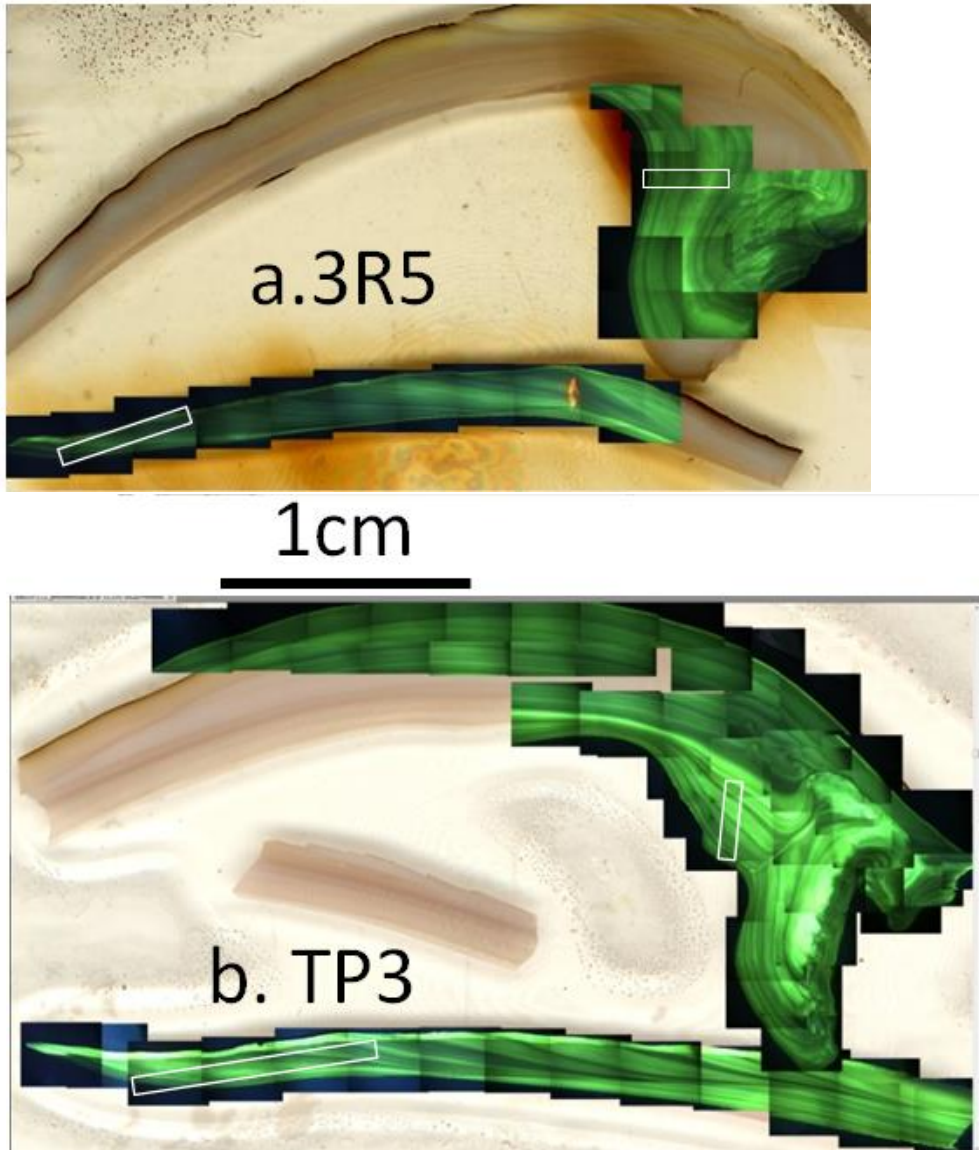
Figure IV-2. Cathodoluminescence (CL) image photomosaics. ImageJ profiles were taken from within the white rectangles lengthwise.

using ImageJ are also presented in Figure IV-1. CL brightness correlates with Mn/Ca values measured by ICP-MS in all shell regions (Table IV-1).

Discussion

Differentiating between environmental and biological controls on shell chemistry depends on how environmental variables influence biological variables. At least three of the four transects show correlations between shell Sr/Ca, Mn/Ca, and δ^{13}C. This could be interpreted as covariance in the Sr/Ca, Mn/Ca, and $\delta^{13}C_{DIC}$ of Brazos River water. However similar mollusk studies indicate that there is a significant chance of at least some metabolic control on mussel shell chemistry, particularly with Sr/Ca (Gillikin et al., 2005; Carré et al., 2006; Gentry et al., 2008; Izumida et al., 2011).

Aside from simply comparing shell and environmental records, inter-shell correlation can also potentially discriminate between environmental and biological controls on shell chemistry. Mussel metabolic rate, particularly the energy consumption in the mantle tissue, is thought to influence shell chemistry and this effect may vary along the mantle from the anterior to ventral margin to posterior regions of the shell (Klein et al., 1996). Furthermore, freshwater mussels sometimes regulate extrapallial fluid trace metal concentrations more strictly than marine bivalves (Wada and Fujinuki, 1976). Such chemical variability between shell regions, species, and environments has not been adequately described.

71

We found no consistent relationships between growth rate and shell chemistry, results similar to those of Klein et al. (1996). Shell growth rate, however, is an imperfect measure of metabolic rate because 1) fine-scale growth rate measurements tend to be imprecise, 2) linear extension rate is a physically arbitrary measure of shell growth (Carré et al., 2006), and 3) many other biological and environmental stresses like reproduction, predation, and pollution can affect mussel metabolic rate independently of shell growth rate.

As with previous studies (Gillikin et al., 2005; Carré et al., 2006; Langlet et al., 2006; Gentry et al., 2008; Izumida et al., 2011), we found a positive relationship between Sr/Ca and temperature. This contrasts with abiotic aragonite precipitate experiments in marine waters (Kinsman and Holland, 1969). It is widely concluded that the positive relationship between Sr/Ca and temperature in aragonitic mollusks are driven by metabolic rate, which can be influenced by water temperature (Gillikin et al., 2005; Carré et al., 2006; Langlet et al., 2006; Izumida et al., 2011). There is a significant correlation between Sr/Ca and %LW (proportion of flow from Whitney dam releases) in three of four transects (Table IV-1) and %LW generally covaries with temperature ($r = 0.515$, $n = 119$, $p < 0.05$). Because %LW rises with summer temperatures and hydropower production and it falls with winter storms and runoff in the Brazos watershed, the relationship with shell Sr/Ca and temperature may signify common seasonal pacing between %LW and shell Sr/Ca. Importantly, Sr/Ca in mollusk shells shows a commonly observed metabolic relationship with temperature rather than following the expected equilibrium relation with temperature, which would result in an

inverse relationship (Kinsman and Holland, 1969). While water source Sr/Ca should have an influence on shell Sr/Ca, evidence for metabolic control paced by temperature weakens the importance of water source influence on shell Sr/Ca in this study. Addition data are needed to constrain the Sr/Ca ratios associated with different sources of water in the Brazos River watershed.

The inter-shell correlations (Table IV-1) suggest there was strong environmental control on shell $\delta^{13}C$ in the ventral margin. Lack of inter-shell $\delta^{13}C$ correlation for the INL transects may be due to the lower time resolution in the INL than the VM. Because the Lake Whitney water itself tends to be higher in $\delta^{13}C_{DIC}$ values than the Brazos River water downstream (Zeng et al., 2011), the consistent correlations between $\delta^{13}C_{shell}$ and %LW (Table IV-1) supports the conclusion that $\delta^{13}C_{shell}$ is significantly influenced by Brazos River $\delta^{13}C_{DIC}$ (CHAPTER III). Studies comparing Brazos shell and DIC $\delta^{13}C$ are needed to confirm this interpretation. McConnaughey and Gillikin (2008) reviewed carbon isotope studies of mollusk shells and suggested that on average about 10% of shell carbonate comes from metabolic DIC (Gillikin et al., 2006; Lorrain et al., 2004), although occasionally the metabolic contribution to total shell carbon can be less or much greater than 10% (Dillaman and Ford, 1982; Tanaka et al., 1986). Dettman et al. (1999) found offsets of up to -9‰ from equilibrium values in freshwater mussels in Michigan, and they suggested this may be due to reproductive investment, however the timing and energetics of brooding and gametogenesis in North American freshwater mussels can vary tremendously (Haag, 2012). While the possibility remains that covariance in $\delta^{13}C_{shell}$ and %LW is not causal but rather a coincidence of metabolic and

environmental patterns, the $\delta^{13}C_{shell}$ signal is probably primarily environmental, based on the combination of inter-shell correlations and %LW data. Poor correlation between $\delta^{13}C_{shell}$ and %LW only in 3R5INL could be explained by 1) greater biological influence on INL than in the ONL, or 2) error in our chronologies.

As with the direct comparison between shell trace elements and water temperature, EC, %LW, and Q, the inter-shell correlations do not indicate consistent strong environmental control on shell Mn/Ca, Mg/Ca, or Ba/Ca. Because Sr/Ca and $\delta^{13}C_{shell}$ covary with seasonal variables and they correlated with Mn/Ca, then Mn/Ca may also be subject to significant environmental control. The relationships between Ba/Ca and Mn/Ca in only the INL transects suggests that there may be differences in how the INL and ONL are formed, and this could be due to differences in extrapallial fluid chemistry between the two regions (Yoshioka and Terai, 1993). The negative relationships between Ba/Ca and $\delta^{13}C$ in TP3 but not in 3R5 suggest that Ba/Ca patterns in these mussel shells are primarily biologically controlled. Some studies have associated high shell Mn/Ca and Ba/Ca values with heightened primary productivity (Stecher et al., 1996; Vander Putten et al., 2000; Lazareth et al., 2003). Langlet et al. (2006) indicates that temperature is mainly responsible for Mn/Ca in a population of French Mediterranean estuarine oysters. Alternatively, watershed lithology or dissolved oxygen concentrations could control freshwater mussel Mn/Ca (Nyström et al., 1996). I suggest that Mn/Ca in these shells is influenced by a combination of environmental and biological factors, paced by yearly temperature cycles that influence metabolic rate but not directly controlled by temperature nor arbitrarily controlled by mussel biology.

Gillikin et al. (2005) and Carré et al. (2006) discuss possible mechanisms for metal ion sorting between mantle tissue and the extrapallial fluid. This biological effect may act on Mn/Ca in a similar way to Sr/Ca in some shells.

The apparent Sr/Ca, Mn/Ca, and Ba/Ca cycles in 3R5 are not seen in TP3 (Figure IV-2). Ignoring water chemistry, I assume that mussel mantle metabolism primarily drives these variables (Gillikin et al., 2005; Carré et al., 2006), and this may vary distinctly between the species or simply the individuals in this study which did not look at a representative number of mussel specimens to make generalizations about species differences. There is lower spatial and temporal resolution for shell chemistry records in the INL than the VM. The offsets in Sr/Ca and in Mn/Ca values between shell regions in both specimens (Figure IV-1) suggest that the INL may undergo a different calcification process from VM (ONL) region. Previous authors have also suggested this. For example, Nyström et al. (1996) observed higher Mn/Ca in INL regions than in ONL regions of bivalves and they cite another study with similar observations (Yoshioka and Terai, 1993).

Cathodoluminescence (CL) can provide a high resolution map of the distribution of Mn^{2+}, which activates green-yellow luminescence when substituted for Ca^{2+} in the aragonite lattice (Barbin, 2000). Correlations between Mn/Ca and CL (Table IV-1) indicate that the micromilling technique used in this study approached the spatial resolution of CL images analyzed for pixel brightness, and this shows that a significant portion of the shell Mn is lattice-bound, although some Mn may be bound in the

proteinaceous shell matrix. Because there are consistent relationships between Mn/Ca and Sr/Ca and between Mn and CL, Mn, Sr, Ca distributions in the shell mineral, and possibly the organic matrix, may be controlled by some of the same fundamental processes. The inconsistencies between CL and light banding patterns in these shells indicate that different processes are responsible for these types of banding in these shells. If future research determines what is responsible for Mn/Ca in common Brazos River mussel shells (e.g., dissolved oxygen, chlorophyll), then CL can be used in conjunction with oxygen isotope chronologies to reconstruct that environmental variable. For future research, I suggest keeping records of Brazos River $\delta^{13}C_{DIC}$, dissolved oxygen, chlorophyll, and dissolved Sr/Ca and Mn/Ca ratios.

Conclusions

In Brazos River freshwater mussels studied here, Sr/Ca, Mn/Ca, and $\delta^{13}C_{shell}$ generally covary, with some exceptions. $\delta^{13}C_{shell}$ is likely driven by water source, and Sr/Ca is likely driven by shell metabolic rate, which may covary with water temperature as in previous studies, while Mn/Ca may be linked to a more intricate combination of metabolic rate, water source, dissolved oxygen, and primary productivity, and temperature. Since Mn/Ca and Ba/Ca covary in three of four shell transects, primary productivity, commonly interpreted to drive Ba/Ca variation in shells, may influence shell Mn/Ca. Sr and Mn are more concentrated in the inner nacreous layer than the ventral margins of the shells, the modes of calcification and perhaps mantle metabolic

rate may differ between these shell regions. Cathodoluminescence microscopy confirms that Mn variations reflect variations in lattice-bound Mn, and not organic-matrix bound Mn.

CHAPTER V

CONCLUSIONS

The Lake Whitney and Brazos River (April-December) δ^{18}O vs. δD data fall on a regression line that is both an evaporation line and a mixing line. Isotope data and modeling from Brazos River water, combined with flow data, indicate that gaining stream conditions are more likely during low flow with low LW contributions to flow. Modeled evaporative Δ^{18}O and measured δ^{18}O of Lake Whitney, the Little River, and the Brazos Alluvium Aquifer (measured previously by Chowdhury et al., 2010) are well constrained for estimating flow contributions from these components using a basic mixing equation (Equation 7). Brazos River isotope values suggest that significant evaporation can take place in the flowing main channel portion of a river. Peak drought conditions may accentuate reservoir discharge dominance in regulated rivers, when baseflow dominance would be expected in a similar undammed river. Estimates of Δ^{18}O$_{RIV-PPT}$ ranged from 0.9‰ for a small creek, to 2.7‰ for a large river, to 3.7‰ in Lake Whitney. This is consistent with previous research on Δ^{18}O$_{RIV-PPT}$ in North America (Kendall and Coplen, 2001; Dutton et al., 2005).

The river water isotope and temperature records can be extended to freshwater mussels to develop a shell chronometer and evaluate the degree to which the shells record environmental conditions. The δ^{18}O$_{SHELL}$ from all four modern specimens show similar values and trends with shell growth and in intra-shell comparisons between the inner nacreous and outer nacreous regions regardless of species. This indicates that

$\delta^{18}O_{SHELL}$ is a valid chronometer, although the inner nacreous layer did not capture as much of the extreme $\delta^{18}O$ values as the ventral margin. We observed consistent intra-shell and inter-shell $\delta^{13}C$ trends. This may be evidence upstream dam releases from Lake Whitney strongly influencing $\delta^{13}C_{DIC}$. Clumped isotope temperatures of shell growth layers can be used to determine what shell segments grew in which season. The use of clumped isotopes as corroborating evidence improves the accuracy of sclerochronology in an environmental study where $\delta^{18}O_{SHELL}$ records are too difficult to interpret alone due to 1) opposing action of temperature and $\delta^{18}O$ of the water on shell records, and 2) variable shell growth rate. Growth chronologies indicate similar growth patterns and winter growth hiatuses between species. While shell isotope values cannot be used to quantify discharge, $\delta^{18}O_{SHELL}$ can still be used to reconstruct discharge variability and to identify major flow events, as well as reconstruct salinity and water source variability, indicating that mussel shells can be useful for paleoenvironment reconstruction. The historical Threeridge shell (*A. plicata*) collected prior to Brazos River dam construction may reflect temperature-driven $\delta^{18}O_{SHELL}$ cycles, but higher resolution clumped isotope measurements should be taken to test this. More historical specimens are needed to test whether the lower $\delta^{18}O_{SHELL}$ values in the 100-year-old Threeridge specimen (H3R) than in the modern shells indicate lower $\delta^{18}O_{WATER}$ values in the Brazos River before dams were constructed. Identical $\delta^{13}C$ values between historical and modern shells indicates that the opposing actions of dam construction and anthropogenic CO_2. Carbon isotope values are consistently significantly lower in *Cyrtonaias tampicoensis* than *Amblema*

plicata. This may be evidence of differences in the rate of incorporation of metabolic carbon in shells between the two species.

In Brazos River freshwater mussels studied here, Sr/Ca, Mn/Ca, and $\delta^{13}C_{shell}$ generally covary, with some exceptions. $\delta^{13}C_{shell}$ is likely driven by water source, and Sr/Ca is likely driven by shell metabolic rate, which may covary with water temperature as in previous studies, while Mn/Ca may be linked to a more intricate combination of metabolic rate, water source, dissolved oxygen, and primary productivity, and temperature. Since Mn/Ca and Ba/Ca covary in three of four shell transects, primary productivity, commonly interpreted to drive Ba/Ca variation in shells, may influence shell Mn/Ca. Sr and Mn are more concentrated in the inner nacreous layer than the ventral margins of the shells, the modes of calcification and perhaps mantle metabolic rate may differ between these shell regions. Cathodoluminescence microscopy confirms that Mn variations reflect variations in lattice-bound Mn, and not organic-matrix bound Mn.

REFERENCES

Barbin, V., 2000, Cathodoluminescence of carbonate shells: biochemical vs diagenetic process, Cathodoluminescence in Geosciences, Springer, p. 303-329.

Böhm, F., Joachimski, M., Lehnert, H., Morgenroth, G., Kretschmer, W., Vacelet, J., and Dullo, W.-C., 1996, Carbon isotope records from extant Caribbean and South Pacific sponges: Evolution of $\delta^{13}C$ in surface water DIC: Earth and Planetary Science Letters, v. 139, no. 1, p. 291-303.

Boulton, A. J., Findlay, S., Marmonier, P., Stanley, E. H., and Valett, H. M., 1998, The functional significance of the hyporheic zone in streams and rivers: Annual Review of Ecology and Systematics, v. 29, p. 59-81.

Burns, D., 2002, Stormflow-hydrograph separation based on isotopes: the thrill is gone— what's next?: Hydrological Processes, v. 16, no. 7, p. 1515-1517.

Carré, M., Bentaleb, I., Bruguier, O., Ordinola, E., Barrett, N. T., and Fontugne, M., 2006, Calcification rate influence on trace element concentrations in aragonitic bivalve shells: Evidences and mechanisms: Geochimica et Cosmochimica Acta, v. 70, no. 19, p. 4906-4920.

Carroll, M., Romanek, C., and Paddock, L., 2006, The relationship between the hydrogen and oxygen isotopes of freshwater bivalve shells and their home streams: Chemical Geology, v. 234, no. 3-4, p. 211-222.

Carroll, M., and Romanek, C. S., 2008, Shell layer variation in trace element concentration for the freshwater bivalve *Elliptio complanata*: Geo-Marine Letters, v. 28, no. 5-6, p. 369-381.

Castro, M. C., Stute, M., and Schlosser, P., 2000, Comparison of ^{4}He ages and ^{14}C ages in simple aquifer systems: implications for groundwater flow and chronologies: Applied Geochemistry, v. 15, no. 8, p. 1137-1167.

Chowdhury, A. H., 2004, Hydraulic Interaction Between Groundwater, Brazos River and Oxbow Lakes: Evidences from Chemical and Isotopic Compositions, Brazos River Basin, Texas, Groundwater Resources Division, Texas Water Development Board.

Chowdhury, A., Osting, T., Furnans, J., Mathews, R., 2010, Groundwater-Surface Water Interaction in the Brazos River Basin: Evidence from Lake Connection History

and Chemical and Isotopic Compositions: Texas Water Development Board Report, v. 375, August, 61 p.

Craig, H., 1961, Isotopic variations in meteoric waters: Science, no. 133, p. 1702-1703.

Craig H., Gordon, LI., 1965, Deuterium and oxygen 18 variations in the ocean and the marine atmosphere, Symposium on Marine Geochemistry, Narraganset Marine Laboratory, University of Rhode Island Publication, 3:277-374.

Criss, R. E., 1999, Principles of stable isotope distribution, Oxford Univ. Press. 264 p.

Criss, R. E., Davisson, M. L., and Kopp, J. W., 2001, Nonpoint sources in the lower Missouri River: Journal-American Water Works Association, v. 93, no. 2, p. 112-122.

Cronin, J. G., and Wilson, C. A., 1967, Ground water in the flood-plain alluvium of the Brazos River, Whitney Dam to vicinity of Richmond, Texas, Texas Water Development Board, 70 p.

Dansgaard, W., 1964, Stable isotopes in precipitation: Tellus, v. 16, no. 4, p. 436-468.

Defliese, W. F., Hren, M. T., and Lohmann, K. C., 2015, Compositional and temperature effects of phosphoric acid fractionation on Δ_{47} analysis and implications for discrepant calibrations: Chemical Geology, v. 396, p. 51-60.

Dennis, K. J., Affek, H. P., Passey, B. H., Schrag, D. P., and Eiler, J. M., 2011, Defining an absolute reference frame for 'clumped' isotope studies of CO_2: Geochimica et Cosmochimica Acta, v. 75, no. 22, p. 7117-7131.

Dettman, D. L., and Lohmann, K. C., 1993, Seasonal Change in Paleogene Surface Water $\delta^{18}O$: Fresh-Water Bivalves of Western North America: Climate change in continental isotopic records, p. 153-163.

Dettman, D. L., and Lohmann, K. C., 1995, Microsampling Carbonates for Stable Isotope and Minor Element Analysis: Physical Separation of Samples on a 20 Micrometer Scale: Research Methods Paper: Journal of Sedimentary Research, v. 65, no. 3.

Dettman, D. L., Reische, A. K., and Lohmann, K. C., 1999, Controls on the stable isotope composition of seasonal growth bands in aragonitic fresh-water bivalves (Unionidae): Geochimica et Cosmochimica Acta, v. 63, no. 7, p. 1049-1057.

Dettman, D. L., Flessa, K. W., Roopnarine, P. D., Schöne, B. R., and Goodwin, D. H., 2004, The use of oxygen isotope variation in shells of estuarine mollusks as a quantitative record of seasonal and annual Colorado River discharge: Geochimica et Cosmochimica Acta, v. 68, no. 6, p. 1253-1263.

Dillaman, R., and Ford, S., 1982, Measurement of calcium carbonate deposition in molluscs by controlled etching of radioactively labeled shells: Marine Biology, v. 66, no. 2, p. 133-143.

Dodd, J. R., 1967, Magnesium and strontium in calcareous skeletons: a review: Journal of Paleontology, p. 1313-1329.

Dunbar, J. A., Amidu, S. A., and Allen, P. M., 2008, A Study Of Seasonal Salinity Variation In Lake Whitney, Texas Using Continuous Resistivity Profiling, in Proceedings 21st EEGS Symposium on the Application of Geophysics to Engineering and Environmental Problems. Marine and Beach Geophysics session II.

Dutton, A., Wilkinson, B. H., Welker, J. M., Bowen, G. J., and Lohmann, K. C., 2005, Spatial distribution and seasonal variation in $^{18}O/^{16}O$ of modern precipitation and river water across the conterminous USA: Hydrological Processes, v. 19, no. 20, p. 4121-4146.

Dworkin, S., 2003, The hydrogeochemistry of the Lake Waco drainage basin, Texas: Environmental geology, v. 45, no. 1, p. 106-114.

Elliot, M., Welsh, K., Chilcott, C., McCulloch, M., Chappell, J., and Ayling, B., 2009, Profiles of trace elements and stable isotopes derived from giant long-lived *Tridacna gigas* bivalves: potential applications in paleoclimate studies: Palaeogeography, Palaeoclimatology, Palaeoecology, v. 280, no. 1, p. 132-142.

Epstein, S., Buchsbaum, R., Lowenstam, H. A., and Urey, H. C., 1953, Revised carbonate-water isotopic temperature scale: Geological Society of America Bulletin, v. 64, no. 11, p. 1315-1326.

Fette, M., Kipfer, R., Schubert, C., Hoehn, E., and Wehrli, B., 2005, Assessing river–groundwater exchange in the regulated Rhone River (Switzerland) using stable isotopes and geochemical tracers: Applied geochemistry, v. 20, no. 4, p. 701-712.

Gentner, H. W., and Hopkins, S. H., 1966, Changes in the trematode fauna of clams in the Little Brazos River, Texas: The Journal of parasitology, p. 458-461.

Gentry, D. K., Sosdian, S., Grossman, E. L., Rosenthal, Y., Hicks, D., and Lear, C. H., 2008, Stable Isotope and Sr/Ca Profiles From the Marine Gastropod Conus ermineus: Testing a Multiproxy Approach For Inferring Paleotemperature and Paleosalinity: Palaios, v. 23, no. 4, p. 195-209.

Gibson, J., and Edwards, T., 2002, Regional water balance trends and evaporation-transpiration partitioning from a stable isotope survey of lakes in northern Canada: Global Biogeochemical Cycles, v. 16, no. 2, p. 10-14.

Gibson, J., and Reid, R., 2010, Stable isotope fingerprint of open-water evaporation losses and effective drainage area fluctuations in a subarctic shield watershed: Journal of Hydrology, v. 381, no. 1, p. 142-150.

Gillikin, D. P., Lorrain, A., Navez, J., Taylor, J. W., André, L., Keppens, E., Baeyens, W., and Dehairs, F., 2005, Strong biological controls on Sr/Ca ratios in aragonitic marine bivalve shells: Geochemistry, Geophysics, Geosystems, v. 6, no. 5, 16p.

Gillikin, D. P., Lorrain, A., Bouillon, S., Willenz, P., and Dehairs, F., 2006, Stable carbon isotopic composition of *Mytilus edulis* shells: relation to metabolism, salinity, δ^{13}C DIC and phytoplankton: Organic Geochemistry, v. 37, no. 10, p. 1371-1382.

Goewert, A., Surge, D., Carpenter, S. J., and Downing, J., 2007, Oxygen and carbon isotope ratios of *Lampsilis cardium* (Unionidae) from two streams in agricultural watersheds of Iowa, USA: Palaeogeography, Palaeoclimatology, Palaeoecology, v. 252, no. 3, p. 637-648.

Gonfiantini, R., 1986, Environmental isotopes in lake studies: Handbook of environmental isotope geochemistry, v. 2, p. 113-168.

Gonfiantini, R., Stichler, W., and Rozanski, K., 1995, Standards and intercomparison materials distributed by the International Atomic Energy Agency for stable isotope measurements.

Grossman, E. L., and Ku, T.-L., 1986, Oxygen and carbon isotope fractionation in biogenic aragonite: temperature effects: Chemical Geology: Isotope Geoscience section, v. 59, p. 59-74.

Haag, W. R., and Commens-Carson, A. M., 2008, Testing the assumption of annual shell ring deposition in freshwater mussels: Canadian Journal of Fisheries and Aquatic Sciences, v. 65, no. 3, p. 493-508.

Haag, W. R., 2009, Extreme longevity in freshwater mussels revisited: sources of bias in age estimates derived from mark-recapture experiments: Freshwater Biology, v. 54, no. 7, p. 1474-1486.

Haag, W. R., and Rypel, A. L., 2011, Growth and longevity in freshwater mussels: evolutionary and conservation implications: Biol Rev Camb Philos Soc, v. 86, no. 1, p. 225-247.

Haag, W. R., 2012, North American freshwater mussels: natural history, ecology, and conservation, Cambridge University Press, 538 p.

Henkes, G. A., Passey, B. H., Wanamaker, A. D., Grossman, E. L., Ambrose, W. G., and Carroll, M. L., 2013, Carbonate clumped isotope compositions of modern marine mollusk and brachiopod shells: Geochimica et Cosmochimica Acta, v. 106, p. 307-325.

Horita, J., and Wesolowski, D. J., 1994, Liquid-vapor fractionation of oxygen and hydrogen isotopes of water from the freezing to the critical temperature: Geochimica et Cosmochimica Acta, v. 58, no. 16, p. 3425-3437.

Hucks Sawyer, A., Bayani Cardenas, M., Bomar, A., and Mackey, M., 2009, Impact of dam operations on hyporheic exchange in the riparian zone of a regulated river: Hydrological Processes, v. 23, no. 15, p. 2129-2137.

Hughes, C., Stone, D., Gibson, J., Sadek, M., Cendón, D., Hankin, S., Hollins, S., and Morrison, T., 2012, Stable Water Isotope Investigation of the Barwon-Darling River System, Australia: Creation of the Global Network of Isotopes in Rivers (GNIR), IAEA-TECDOC-1673, p. 97-110.

Hui, Q., Mengyao, L., Yadong, J., Bingchao, Y., and Zhenhong, Z., 2007, Changes of $\delta^{18}O$ and δD along the Dousitu River, Inner Mongolia, China, and their evidence of river water evaporation: Aquatic Geochemistry, v. 13, no. 2, p. 127-142.

IAEA, 1992, Statistical Treatment of Data on Environmental Isotopes in Precipitation, Technical Reports Series No. 331: Vienna, Austria, International Atomic Energy Agency, 781 p.

Ivany, L. C., Wilkinson, B. H., Lohmann, K. C., Johnson, E. R., McElroy, B. J., and Cohen, G. J., 2004, Intra-annual isotopic variation in Venericardia bivalves: Implications for early Eocene temperature, seasonality, and salinity on the US Gulf Coast: Journal of Sedimentary Research, v. 74, no. 1, p. 7-19.

Izumida, H., Yoshimura, T., Suzuki, A., Nakashima, R., Ishimura, T., Yasuhara, M., Inamura, A., Shikazono, N., and Kawahata, H., 2011, Biological and water chemistry controls on Sr/Ca, Ba/Ca, Mg/Ca and δ^{18}O profiles in freshwater pearl mussel Hyriopsis sp: Palaeogeography, Palaeoclimatology, Palaeoecology, v. 309, no. 3, p. 298-308.

Keating-Bitonti, C. R., Ivany, L. C., Affek, H. P., Douglas, P., and Samson, S. D., 2011, Warm, not super-hot, temperatures in the early Eocene subtropics: Geology, v. 39, no. 8, p. 771-774.

Kinsman, D. J., and Holland, H., 1969, The co-precipitation of cations with CaCO 3—IV. The co-precipitation of Sr^{2+} with aragonite between 16 and 96 C: Geochimica et Cosmochimica Acta, v. 33, no. 1, p. 1-17.

Klein, R. T., Lohmann, K. C., and Thayer, C. W., 1996, Sr/Ca and ^{13}C/^{12}C ratios in skeletal calcite of *Mytilus trossulus*: Covariation with metabolic rate, salinity, and carbon isotopic composition of seawater: Geochimica et Cosmochimica Acta, v. 60, no. 21, p. 4207-4221.

Kendall, C., and McDonnell, J. J., 1999, Isotope tracers in catchment hydrology, Elsevier Science, Amsterdam, 839 p.

Kendall, C., and Coplen, T. B., 2001, Distribution of oxygen-18 and deuterium in river waters across the United States: Hydrological Processes, v. 15, no. 7, p. 1363-1393.

Kerr, E., 2012, Brutal drought depresses agriculture, thwarting US and Texas economies: The Southwest Economy, no. Q4, p. 10-13.

Lambs, L., 2000, Correlation of conductivity and stable isotope ^{18}O for the assessment of water origin in river system: Chemical Geology, v. 164, no. 1, p. 161-170.

Langlet, D., Alunno-Bruscia, M., Rafélis, M., Renard, M., Roux, M., Schein, E., and Buestel, D., 2006, Experimental and natural cathodoluminescence in the shell of *Crassostrea gigas* from Thau lagoon (France): ecological and environmental implications: Marine Ecology Progress Series, v. 317, p. 143-156.

Larkin, T., and Bomar, W., 1983, Climate atlas of Texas: Texas Department of Water Resources, LP-192, 157 p.

Lazareth, C., Vander Putten, E., André, L., and Dehairs, F., 2003, High-resolution trace element profiles in shells of the mangrove bivalve *Isognomon ephippium*: a

record of environmental spatio-temporal variations?: Estuarine, Coastal and Shelf Science, v. 57, no. 5, p. 1103-1114.

Lorrain, A., Paulet, Y.-M., Chauvaud, L., Dunbar, R., Mucciarone, D., and Fontugne, M., 2004, δ^{13}C variation in scallop shells: increasing metabolic carbon contribution with body size?: Geochimica et Cosmochimica Acta, v. 68, no. 17, p. 3509-3519.

Lydeard, C., Cowie, R. H., Ponder, W. F., Bogan, A. E., Bouchet, P., Clark, S. A., Cummings, K. S., Frest, T. J., Gargominy, O., and Herbert, D. G., 2004, The global decline of nonmarine mollusks: BioScience, v. 54, no. 4, p. 321-330.

McConnaughey, T. A., and Gillikin, D. P., 2008, Carbon isotopes in mollusk shell carbonates: Geo-Marine Letters, v. 28, no. 5-6, p. 287-299.

Moore, G., Edgar, C., Vogel, J., Washington-Allen, R., March, R., and Zehnder, R., Widespread Tree Mortality from the 2011 Texas Drought: Consequences for Forest Structure and Carbon Stocks, in Proceedings AGU Fall Meeting Abstracts 2013, Volume 1, p. 0599.

Munster, C., Mathewson, C. C., and Wrobleski, C., 1996, The Texas A&M University Brazos River hydrogeologic field site: Environmental & Engineering Geoscience, v. 2, no. 4, p. 517-530.

Nativ, R., and Riggio, R., 1990, Precipitation in the southern High Plains: meteorologic and isotopic features: Journal of Geophysical Research: Atmospheres (1984–2012), v. 95, no. D13, p. 22559-22564.

Neves, R. J., and Moyer, S. N., 1988, Evaluation of techniques for age determination of freshwater mussels (Unionidae): American Malacological Bulletin, v. 6, no. 2, p. 179-188.

Nicot, J.-P., Gross, B., Walden, S., and Baier, R., 2007, Self-sealing evaporation ponds for desalination facilities in Texas, Texas Water Development Board, under Contract No. 2005-483-027, 248p.

Nielsen-Gammon, J. W., 2012, The Changing Climate of Texas, in Schmandt, J. N., Gerald R.; Clarkson, Judith, ed., The Impact of Global Warming on Texas: Austin, University of Texas Press, p. 39-68.

Nyström, J., Dunca, E., Mutvel, H., and Lindh, U., 1996, Environmental history as reflected by freshwater pearl mussels in the River Vramsån, southern Sweden: Ambio, p. 350-355.

Quay, P., Sonnerup, R., Westby, T., Stutsman, J., and McNichol, A., 2003, Changes in the $^{13}C/^{12}C$ of dissolved inorganic carbon in the ocean as a tracer of anthropogenic CO_2 uptake: Global Biogeochemical Cycles, v. 17, no. 1, p. 4-1-4-20.

Randklev, C. R., Johnson, M. S., Tsakiris, E. T., Groce, J., and Wilkins, N., 2013, Status of the freshwater mussel (Unionidae) communities of the mainstem of the Leon River, Texas: Aquatic Conservation: Marine and Freshwater Ecosystems, v. 23, no. 3, p. 390-404.

Richter, B. D., Braun, D. P., Mendelson, M. A., and Master, L. L., 1997, Threats to imperiled freshwater fauna: Conservation Biology, v. 11, no. 5, p. 1081-1093.

Rawson, J., 1967, Study and interpretation of chemical quality of surface waters in the Brazos River basin, Texas: Texas Water Development Board, Report 55, 116 p.

Roark, A., Grossman, E.L., Lebold, J. In Press. Low seasonality in central equatorial Pangea during a late Carboniferous highstand based on high-resolution isotopic records of brachiopod shells: GSA Bulletin.

Schöne, B. R., Oschmann, W., Rössler, J., Castro, A. D. F., Houk, S. D., Kröncke, I., Dreyer, W., Janssen, R., Rumohr, H., and Dunca, E., 2003, North Atlantic Oscillation dynamics recorded in shells of a long-lived bivalve mollusk: Geology, v. 31, no. 12, p. 1037-1040.

Shah, S. D., Houston, N. A., and Braun, C. L., 2007, Hydrogeologic Characterization of the Brazos River Alluvium Aquifer, Bosque County to Fort Bend County, Texas, US Geological Survey.

Stamm, R. G., and Wingard, G. L., USGS Fact Sheet 2004-3141.

Stecher, H., Krantz, D., Lord, C., Luther, G., and Bock, K., 1996, Profiles of strontium and barium in *Mercenaria mercenaria* and *Spisula solidissima* shells: Geochimica et Cosmochimica Acta, v. 60, no. 18, p. 3445-3456.

Strayer, D. L., Downing, J. A., Haag, W. R., King, T. L., Layzer, J. B., Newton, T. J., and Nichols, J. S., 2004, Changing perspectives on pearly mussels, North America's most imperiled animals: BioScience, v. 54, no. 5, p. 429-439.

Surge, D., Lohmann, K. C., and Dettman, D. L., 2001, Controls on isotopic chemistry of the American oyster, *Crassostrea virginica*: implications for growth patterns: Palaeogeography, Palaeoclimatology, Palaeoecology, v. 172, no. 3, p. 283-296.

Swarzenski, P. W., Reich, C., Kroeger, K. D., and Baskaran, M., 2007, Ra and Rn isotopes as natural tracers of submarine groundwater discharge in Tampa Bay, Florida: Marine Chemistry, v. 104, no. 1, p. 69-84.

Tanaka, N., Monaghan, M. C., and Rye, D. M., 1986, Contribution of metabolic carbon to mollusc and barnacle shell carbonate: Nature, v. 320, p. 520-523.

Tufenkji, N., Ryan, J. N., and Elimelech, M., 2002, Peer reviewed: The promise of bank filtration: Environmental science & technology, v. 36, no. 21, p. 422A-428A.

Turco M.J., East J.W., Milburn M.S., 2007, Base flow (1966-2005) and streamflow gain and loss (2006) of the Brazos River, McLennan County to Fort Bend County, Texas: US Department of the Interior, US Geological Survey, Scientific Investigations Report 2007-5286, p. 1-35.

Vander Putten, E., Dehairs, F., Keppens, E., and Baeyens, W., 2000, High resolution distribution of trace elements in the calcite shell layer of modern *Mytilus edulis*: Environmental and biological controls: Geochimica et Cosmochimica Acta, v. 64, no. 6, p. 997-1011.

Versteegh, E. A., Vonhof, H. B., Troelstra, S. R., Kaandorp, R. J., and Kroon, D., 2010a, Seasonally resolved growth of freshwater bivalves determined by oxygen and carbon isotope shell chemistry: Geochemistry, Geophysics, Geosystems, v. 11, n. 8, 16 p.

Versteegh, E. A. A., Vonhof, H. B., Troelstra, S. R., and Kroon, D., 2010b, Can shells of freshwater mussels (Unionidae) be used to estimate low summer discharge of rivers and associated droughts?: International Journal of Earth Sciences, v. 100, no. 6, p. 1423-1432.

Wada, K., and Fujinuki, T., 1976, Biomineralization in bivalve molluscs with emphasis on the chemical composition of the extrapallial fluid: The Mechanisms of Mineralization in Invertebrates and Plants, p. 175-190.

Ward, G. H., 2012, Water Resourcces and Water Supply, in Schmandt, J. N., Gerald R.; Clarkson, Judith, ed., The Impact of Global Warming on Texas: Austin, University of Texas Press, p. 69-95.

Wurbs, R., and Lee, C., 2009, Salinity budget and WRAP salinity simulation studies of the Brazos River/Reservoir System: Texas Water Resources Institute. Available electronically from http://hdl. handle. net/1969, v. 1, p. 90516.

Wurbs, R. A., and Ayala, R. A., 2014, Reservoir evaporation in Texas, USA: Journal of Hydrology, v. 510, p. 1-9.

Yoshioka, S., Terai, M., 1993, Manganese accumulation in freshwater bivalves: Biomineralization, '93, 'Instuitut Oceanographique, Monaco, presentation abstract.

Zarfl, C., Lumsdon, A. E., Berlekamp, J., Tydecks, L., and Tockner, K., 2015, A global boom in hydropower dam construction: Aquatic Sciences, v. 77, no. 1, p. 161-170.

Zeng, F.-W., Masiello, C. A., and Hockaday, W. C., 2011, Controls on the origin and cycling of riverine dissolved inorganic carbon in the Brazos River, Texas: Biogeochemistry, v. 104, no. 1-3, p. 275-291.

Bivariate plots of Mn/Ca vs. Sr/Ca, Mn/Ca vs. Ba/Ca, δ^{13}C vs. Sr/Ca, δ^{13}C vs. Mn/Ca, δ^{13}C vs. %LW (% of discharge from Lake Whitney releases) in TP3INL, TP3VM, 3R5INL, 3R5VM.